



**HAL**  
open science

## Groundwater discharge to coastal streams – A significant pathway for nitrogen inputs to a hypertrophic Mediterranean coastal lagoon

Marine David, Vincent Bailly-Comte, Dominique Munaron, Annie Fiandrino, Thomas Stieglitz

### ► To cite this version:

Marine David, Vincent Bailly-Comte, Dominique Munaron, Annie Fiandrino, Thomas Stieglitz. Groundwater discharge to coastal streams – A significant pathway for nitrogen inputs to a hypertrophic Mediterranean coastal lagoon. *Science of the Total Environment*, 2019, 677, pp.142-155. 10.1016/j.scitotenv.2019.04.233 . hal-02117547

**HAL Id: hal-02117547**

**<https://hal.science/hal-02117547>**

Submitted on 6 May 2019

**HAL** is a multi-disciplinary open access archive for the deposit and dissemination of scientific research documents, whether they are published or not. The documents may come from teaching and research institutions in France or abroad, or from public or private research centers.

L'archive ouverte pluridisciplinaire **HAL**, est destinée au dépôt et à la diffusion de documents scientifiques de niveau recherche, publiés ou non, émanant des établissements d'enseignement et de recherche français ou étrangers, des laboratoires publics ou privés.

1 **Groundwater discharge to coastal streams – a significant pathway for nitrogen inputs to**  
2 **a hypertrophic Mediterranean coastal lagoon**

3 Marine **David**<sup>1,2,3</sup>, Vincent **Bailly-Comte**<sup>2</sup>, Dominique **Munaron**<sup>1</sup>, Annie **Fiandrino**<sup>1</sup>, Thomas  
4 **C. Stieglitz**<sup>3,4</sup>

5 1) Ifremer, UMR MARBEC (IRD, Ifremer, CNRS, Université de Montpellier, CNRS),  
6 Sète, France

7 2) NRE, BRGM, University of Montpellier, Montpellier, France

8 3) CEREGE, Aix-Marseille Université, CNRS, IRD, Coll France, 13545 Aix-en-  
9 Provence, France

10 4) Centre for Tropical Water and Aquatic Ecosystem Research, James Cook University,  
11 Townsville, Queensland 4811, Australia

12 **Highlights**

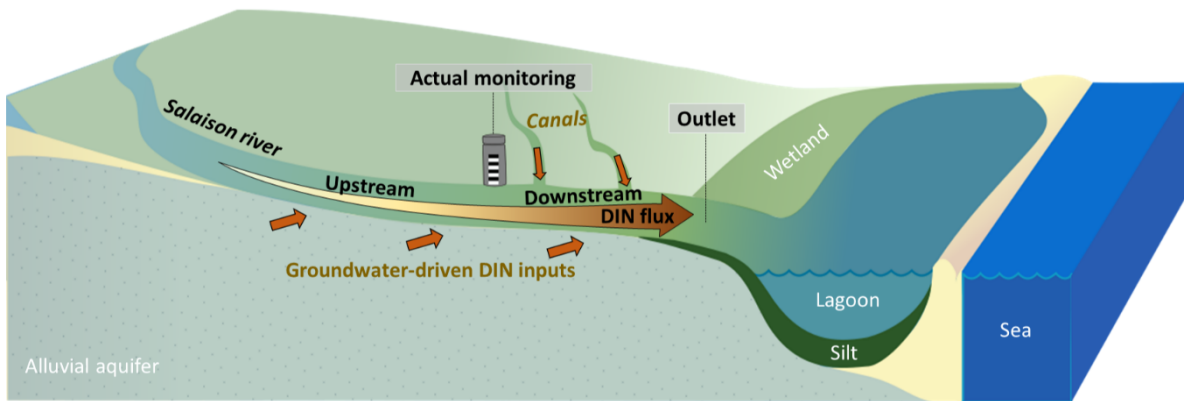
- 13 - Groundwater contribution to nitrogen fluxes was investigated in a major tributary to Or  
14 lagoon  
15 - Groundwater is a major source of dissolved inorganic nitrogen (DIN) for the Salaison  
16 River  
17 - DIN fluxes monitored at the Salaison gauging station are considerably underestimated  
18 - Groundwater driven DIN inputs should be taken into account in coastal lagoons  
19 management actions

20

21

22

23 **Graphical abstract**



24

25 **Abstract**

26 Near-shore and direct groundwater inputs are frequently omitted from nutrient budgets of  
27 coastal lagoons. This study investigated groundwater-driven dissolved inorganic nitrogen  
28 (DIN) inputs from an alluvial aquifer to the hypertrophic Or lagoon, with a focus on the  
29 Salaison River. Piezometric contours revealed that the Salaison hydrogeological catchment is  
30 42% bigger than the surface watershed and hydraulic gradients suggest significant groundwater  
31 discharge all along the stream. Hydrograph separation of the water flow at a gauging station  
32 located 3 km upstream from the Or lagoon combined with DIN historical data enabled to  
33 estimate that groundwater-driven DIN inputs account for 81-87% of the annual total DIN inputs  
34 to the stream upstream from the gauging station. A radon mass balance was performed for the  
35 hydrological cycle 2017-2018 to estimate groundwater inflow into this downstream part of the  
36 stream. Results showed that (1) DIN fluxes increased by a factor 1.1 to 2.3 between the gauging  
37 station and the Salaison outlet, (2) the increase in DIN was due to two groundwater-fed canals  
38 and to groundwater discharge along the stream, the latter represented 63-78% of the water flow.  
39 This study thus highlights the significance of groundwater driven DIN inputs into the Salaison  
40 River, which account for 90% of the annual DIN inputs. This is particularly true in the  
41 downstream part of the river, which, on averages, supplies 48% of total DIN inputs to the river.  
42 These DIN inputs into the Or lagoon were previously not taken into account in the management  
43 of this and other Mediterranean lagoons. The inputs will probably affect restoration processes  
44 for many years due to their residence time in the aquifer. This study throws light on a rarely  
45 documented source of ‘very-nearshore’ groundwater discharge to coastal streams in water and  
46 nutrient budgets of coastal zone ecosystems.

47

48

## 49 **2. Introduction**

50 Transitional water bodies like Mediterranean coastal lagoons are located at the interface  
51 between the continent and the sea, they are productive areas which provide substantial  
52 ecosystem services (Mooney et al., 2009; Newton et al., 2018). In these semi-enclosed water  
53 bodies, the gradient from fresh to saline water creates rich biodiversity which has been  
54 documented and protected for several decades now (Basset et al., 2013). As export to the open  
55 sea is limited, residence time in these water bodies is sufficiently long to enable assimilation  
56 of nutrients by living organisms (Kjerfve and Magill, 1989; Quintana et al., 1998). Coastal  
57 lagoons are thus particularly sensitive to nutrient fluxes resulting from anthropogenic activities  
58 (de Jonge et al., 2002; Newton et al., 2014). Excess nutrient inputs can lead to eutrophication  
59 of the water column, and proliferation of competitive species, thereby upsetting biodiversity  
60 equilibrium and reducing the quality of the water (Cloern 2001; Souchu et al. 2010). Among  
61 nutrient fluxes, the significant impacts of dissolved inorganic nitrogen (DIN) on eutrophication  
62 were already investigated three decades ago (Rimmelin et al., 1998; Taylor et al., 1995).

63 The main sources of DIN contamination investigated in the past are soil leaching from  
64 agricultural land, discharge from wastewater treatment plants (WWTPs), and urban and  
65 industrial effluents (Derolez et al., 2014). Indeed, DIN inputs from streams to coastal zones are  
66 mostly supplied by surface water, which transports agricultural inputs and wastewater  
67 (Meinesz et al., 2013). More recently, groundwater has also been considered as a source of  
68 DIN to the coastal zone (Johannes, 1980; Moore, 2010; Rodellas et al., 2015). These studies  
69 mainly focussed on direct submarine groundwater discharge (Burnett et al., 2006; Rodellas et  
70 al., 2018; Stieglitz et al., 2013) and some demonstrated that inputs from aquifers can  
71 significantly contribute to total coastal DIN inputs (Moore, 2010; Slomp and Van Cappellen,  
72 2004). However, the contributions of groundwater inflow to streams discharging in the  
73 immediate coastal environment has rarely been investigated (Martinez et al., 2015; Peterson et  
74 al., 2010; Santos et al., 2010).

75 The goal of the present study was thus to assess inputs of DIN from a coastal aquifer system to  
76 a stream discharging into the hypertrophic Or lagoon located in the South of France. This  
77 lagoon suffers from recurrent eutrophication which led to a 'bad' ecological status according  
78 to the European Union Water Frame Directive (Symbo, 2017). Inputs of DIN from surface  
79 waters to the lagoon have been significantly reduced by management actions in the past 20  
80 years, mainly thanks to improvements of wastewater treatment plants and to a lesser extent, to  
81 changes in agricultural fertilisation practices. However, despite these actions, no lasting  
82 improvement in the quality of the lagoon water has been observed (Derolez et al., 2017). As  
83 Salaison River is a perennial stream, groundwater inputs help maintain the water flow in  
84 periods with no rainfall, but the associated DIN fluxes have not previously been studied.  
85 Regional groundwater has high concentrations of DIN, and, given the comparatively long  
86 transit times and associated time lags before discharge, inputs from this coastal aquifer could  
87 be an obstacle to restoring Or lagoon.

88 Different methods are routinely implemented at different scales to study groundwater pathways  
89 to streams or to the coastline:

- 90 (1) At the aquifer scale, piezometric maps are used to identify drainage pathways, but this  
91 method requires a good knowledge of the aquifer geometry and its hydrodynamics  
92 properties (Burnett et al., 2001; Schilling and Wolter, 2007).
- 93 (2) At the surface watershed scale, hydrograph separation of streamflow data enables  
94 surface runoff to be distinguished from groundwater discharge (Chapman, 1999;  
95 Eckhardt, 2005; Schilling and Wolter, 2001). However, in coastal rivers, most gauging  
96 stations collecting such data are located a few kilometers upstream from the outlet to  
97 avoid the influence of the tide, which can lead to the underestimation of total inputs to  
98 the coastline (Santos et al., 2010).
- 99 (3) At a smaller scale, natural groundwater tracers like radon and radium are widely used  
100 to locate and quantify groundwater discharge into streams (Cook et al., 2003; Mullinger  
101 et al., 2007). High concentrations of these radionuclides are naturally found in  
102 groundwater whereas low concentrations are found in surface waters, making them  
103 efficient tracers of groundwater origin (Burnett and Dulaiova, 2003; Charette et al.,  
104 2001). Groundwater flow can be quantified using a mass balance along the stream  
105 (Cook et al., 2006; Peterson et al., 2010).

106 Even though combining approaches to improve our knowledge of the interactions between the  
107 aquifer and the coast would seem obvious (Burnett et al., 2001; Martinez et al., 2015), in the  
108 past, these methods were usually applied separately (Banks et al., 2011; Burnett et al., 2006;  
109 Menció et al., 2014). In the present study, the three approaches were combined to locate and  
110 quantify groundwater contribution to DIN inputs in Salaison River. In particular, groundwater  
111 inputs were investigated in the section of the stream close to the outlet, downstream from the  
112 Salaison gauging station. The three methods were combined to (i) obtain a more holistic view  
113 of the hydrogeological functioning of this coastal stream than is possible using a single method,  
114 (ii) estimate the groundwater contribution to the Or lagoon via the Salaison River, and (iii)  
115 assess more accurate DIN fluxes to the Or lagoon than estimated at the Salaison River gauging  
116 station.

### 117 **3. Material and methods**

#### 118 **3.1. Study sites**

##### 119 **3.1.1. Or lagoon**

120 The Or lagoon is located southeast of the city of Montpellier on the French Mediterranean coast  
121 (**Fig. 1a**). The surface area of the lagoon is 29.6 km<sup>2</sup> and the average depth is 1 m. In addition  
122 to the presence of an east-west salinity gradient, the lagoon is subject to marked interannual  
123 variations in salinity (from 2 to 35 psu). The northern bank of the lagoon is at the edge of 20  
124 km<sup>2</sup> of wetlands which have been the subject of major land reclamations actions. The Or lagoon  
125 watershed covers 410 km<sup>2</sup>, and has a flat landform rising from 0 (sea level) to 193 m asl (Blaise  
126 et al., 2008). The area is characterised by a typical Mediterranean climate. Precipitation is very  
127 low in summer, but intense rainfall events in spring and autumn can cause serious flooding.  
128 Annual average precipitation ranges from 600 mm in the southern part of the watershed to 750  
129 mm in the northern part (Aquascop, 2013). The area is urbanized but agriculture still represents  
130 a major land use with intensively managed vineyards, market gardening, orchards and cereal  
131 crops. These activities have led to significant nutrient loading of the underlying aquifer, for

132 example, nitrate concentrations reach  $1600 \mu\text{mol.L}^{-1}$  (i.e.  $100 \text{ mg}(\text{NO}_3)/\text{L}$ ) in the eastern part  
133 of the aquifer (ADES database <http://ades.eaufrance.fr>).

134 The Or lagoon lies on a Holocene clay and clayey sand formation and is bound to the north by  
135 the coastal plain of Mauguio-Lunel (**Fig. 1a**). The adjacent Villafranchien aquifer is formed by  
136 the most recent layers of alluvial and colluvial deposits from the Pliocene and the Holocene,  
137 overlying a cretaceous and Jurassic limestone bedrock (Blaise et al., 2008). This aquifer  
138 outcrops over  $252 \text{ km}^2$ , it is limited to the west by the Lez River and to the east by the Vidourle  
139 River, and is partly fed by limestone (karst aquifer) along its north boundary. The aquifer is  
140 unconfined, except downstream at the edge of the lagoon where it becomes confined as it  
141 expands under Holocene silt. The presence of impermeable silt and clay from the Holocene  
142 prevents direct exchanges of water between the aquifer and the lagoon, but to date, little is  
143 known about the possible connections through the perennial streams which drain the aquifer  
144 (Blaise et al., 2008).

### 145 **3.1.2. Salaison River**

146 The Or lagoon is supplied with freshwater from natural streams and artificial canals (**Fig. 1a**).  
147 In the eastern watershed, the Lunel and Rhône to Sète canals bring water from the eastern  
148 alluvial plain. The present study focusses on the northern part of the watershed, where natural  
149 streams flow into the lagoon. Five main rivers and ten temporary streams flowing in a north-  
150 west south-east direction discharge into the Or lagoon. The Salaison River is one of the main  
151 tributaries flowing into the lagoon, which accounts for 59% (2015-2016) of the total freshwater  
152 supplied by the streams in the watershed (Colin et al., 2017). The Salaison River drains a  $66$   
153  $\text{ km}^2$  watershed which corresponds to 17% of the northern watershed of the Or lagoon. The  
154 source of the river is located on the northern Cretaceous limestone and, for its last nine  
155 kilometers, it flows over the Villafranchien aquifer.

156 The Salaison River used to receive effluents from four waste water treatment plants (WWTPs)  
157 (St Vincent de Barbeyrargues, St Aunes, Vendargues, Mauguio, with a total of 53 800  
158 population equivalent) (Aquascop, 2013). In order to reduce inputs to Salaison and Or lagoon,  
159 St Vincent de Barbeyrargues WWTP (800 population equivalent) has not released any  
160 discharge into the Salaison since 2010, and the three other WWTP outlets were removed from  
161 the river between 2008 and 2011 (Symbo, 2014). Since then, diffuse surface and groundwater  
162 flows have been the sources of nitrogen inputs into the stream. In addition, the river is fed in  
163 its downstream part by two canals, one of which (Balaurie) used to receive effluent from the  
164 Vendargues WWTP (6 000 population equivalent) before it was removed and the other  
165 (Roubine) was used for urban and storm water drainage (**Fig. 1b**).

### 166 **3.2. Groundwater catchment of the Salaison river**

167 A piezometric survey of the aquifer was carried out to identify the Salaison groundwater  
168 catchment, i.e. the area of the aquifer that interacts with the stream. Water levels were measured  
169 at 18 piezometers in high water table conditions on May 2<sup>nd</sup> and 3<sup>rd</sup> 2018 (**Fig. 1b**). Relative  
170 water level data were combined with the stream elevation and a digital elevation model to  
171 obtain the piezometric contours around the Salaison River by interpolation in ArcGIS.

172 Groundwater contours based on water table crests on both sides of the Salaison River were  
173 used to delineate the Salaison's groundwater catchment.

### 174 **3.3. Salaison gauging station**

175 Since 1986, stream water flow has been monitored through high-frequency limnometric  
176 measurements made by the Regional Department for Environment, Development and Housing  
177 (French acronym DREAL). The gauging station is located 3 km upstream from the outlet to  
178 the lagoon and upstream from the Balaurie and Roubine canals (**Fig .1b**), capturing 75% of its  
179 total watershed (i.e. 50 km<sup>2</sup>). Since 2006, DIN concentrations have been sampled by  
180 management agencies every two weeks under regular monitoring and at greater frequencies  
181 during floods, to assess DIN fluxes at the gauging station.

### 182 **3.4. Combined methods upstream and downstream from the gauging station**

183 In this study, two sections of the stream were distinguished based on the location of the gauging  
184 station: upstream and downstream sections. In the upstream section, the contributions of  
185 groundwater to the total DIN inputs at the gauging station were investigated. In the downstream  
186 section, additional inputs occurring between the gauging station and the Salaison outlet were  
187 also investigated, including the two downstream canals, along with groundwater contribution.

188 In any part of the stream, instantaneous DIN fluxes  $f_X(t)$  (in  $\mu\text{mol}\cdot\text{s}^{-1}$ ) were estimated as the  
189 product of water flow  $Q_X(t)$  (in  $\text{L}\cdot\text{s}^{-1}$ ) and DIN concentration  $[N]_X(t)$  (in  $\mu\text{mol}\cdot\text{L}^{-1}$ ) (eq. 1) :

$$190 \quad f_X(t) = Q_X(t) \cdot [N]_X(t) \quad (1)$$

191 In the rest of the paper, the time increment '(t)' was removed for the purpose of clarity (i.e.  $f_X$ ,  
192  $Q_X$  and  $[N]_X$ ).

193 First, total DIN fluxes were assessed in each section. Then, estimating groundwater driven DIN  
194 fluxes enabled to obtain the groundwater contribution to the total DIN fluxes. The two sections  
195 of the stream were approached differently (**Table 1**):

- 196 - the upstream part was investigated using historical data collected from 2013 to 2018 at  
197 the gauging station, to estimate total DIN fluxes  $f_{\text{station}}$  and groundwater driven DIN flux  
198  $f_{\text{gw}}$  (detailed in section **2.5**),
- 199 - Supplementary field data were collected in the hydrological cycle 2017-2018 for the  
200 downstream section, to estimate additional DIN fluxes  $\Delta f_{\text{downstream}}$  and additional  
201 groundwater driven DIN fluxes  $\Delta f_{\text{gw}}$  using a radon mass balance (detailed in section  
202 **2.6**),

203 Instantaneous DIN fluxes  $f_X$  were integrated over one hydrological year (from September 1<sup>st</sup> to  
204 the following August 31<sup>st</sup>) and converted into tonnes to estimate annual DIN inputs  $F_X$  (in  $\text{tN}\cdot\text{y}^{-1}$ ).  
205 The relative groundwater contribution to the total DIN flux was estimated as the ratio of  
206 groundwater driven DIN flux to total DIN flux.

207 **3.5. Groundwater contribution to DIN fluxes upstream from the Salaison gauging**  
208 **station**

209 **3.5.1. Water flow at the gauging station**

210 Stream water flow data  $Q_{\text{station}}$  at the gauging station (**Fig. 1b**) were extracted for the past five  
211 hydrological cycles from the DREAL database (hydro.eaufrance.fr, station Y3315080, 2013 -  
212 2018) at hourly intervals, taking into account the fact that the Salaison has a fast hydrological  
213 response to rainfall (less than 6 hours between a rainfall event and an increase in flow).

214 **3.5.2. DIN fluxes at the gauging station**

215 Dissolved inorganic nitrogen (DIN) concentrations were extracted from the public water  
216 quality database Naiades (<http://naiades.eaufrance.fr/>). A total of 81 DIN data were collected  
217 from 2013 to 2018 and clustered according to their associated water flow to assess mean  
218 nutrient concentrations for three water flow classes  $[N]_{\text{station}}$  (**Table 2**). The DIN flux at the  
219 gauging station  $f_{\text{station}}$  is obtained using eq. 1 with  $Q_{\text{station}}$  and the associated average DIN class  
220 concentrations  $[N]_{\text{station}}$ . Standard variations in DIN concentrations in each of the three classes  
221 were used to estimate uncertainty.

222 **3.5.3. Groundwater flow at the gauging station**

223 Groundwater flow  $Q_{\text{gw}}$  was obtained from hydrograph separation of the stream water flow  
224  $Q_{\text{station}}$ . The Chapman model (Chapman, 1999) separates fast subsurface flow from base flow,  
225 the latter usually being driven by groundwater. The FlowScreen R package with the function  
226 `bf_oneparam` was used to assess time series of groundwater flow at an hourly time step. The  
227 recession constant was estimated for each hydrological cycle using the ESPERE tool (BRGM,  
228 Lanini et al. 2016), ( $\mu=0.971$ ,  $\sigma=0.019$ ,  $n=5$ ).

229 **3.5.4. Groundwater end-member for DIN concentrations at the gauging station**

230 Three sets of data were collected to determine the groundwater end-member for DIN  
231 concentration at the gauging station  $[N]_{\text{gw}_s}$  :

- 232 - piezometer P4 was sampled for groundwater DIN concentrations on March 8<sup>th</sup>, April  
233 27<sup>th</sup>, May 5<sup>th</sup>, June 25<sup>th</sup> and July 27<sup>th</sup> in 2018. In this study, this well was assumed to be  
234 representative of the groundwater characteristics because of its location close to the  
235 gauging station (**Fig.1b**). In addition, piezometer St Aunes, located upstream of the  
236 Salaison watershed, was sampled on March 8<sup>th</sup>, June 25<sup>th</sup> and July 27<sup>th</sup> in 2018. For  
237 each sample, *in situ* salinity was measured using a multiparameter probe (WTW 3620).
- 238 - past DIN concentrations in groundwater at the P4 piezometer were taken from the  
239 BRGM study in 2006-2007 (Blaise et al., 2008). These past data were compared with  
240 new data to quantify changes in DIN concentrations over the past decade.
- 241 - stream data for DIN concentration and conductivity at the gauging station were also  
242 used to determine the groundwater end-member.



243 **3.6. Groundwater contribution to DIN fluxes downstream from the Salaison gauging**  
244 **station**

245 **3.6.1. Water inflow downstream from the gauging station**

246 **3.6.1.1. Use of a radon and water balance to assess total and groundwater**  
247 **flow**

248 A combined water and radon mass balance was constructed in the downstream part of the  
249 stream using two successive box models (**Fig. 2**) to estimate, for the hydrological cycle 2017-  
250 2018, (1) the additional groundwater discharge  $\Delta Q_{gw}$  and (2) the total additional water flow  
251  $\Delta Q_{downstream}$  discharging between the gauging station and the outlet.

252 The first box for the radon mass balance includes the first 700 m downstream from the gauging  
253 station with the discharge from the Balaurie canal, and the second box, the section from 700 m  
254 to 2000 m, taking the discharge from the Roubine canal into account (**Fig. 1c**). The final section  
255 (2000 m-3000 m downstream from the gauging station) is affected by changes in lagoon water  
256 surface level caused by variations in wind and atmospheric pressure, as indicated by variable  
257 salinity. The last section can consequently not be considered as being in a steady state.  
258 Geological data showed that this section receives a negligible inflow of groundwater due to the  
259 impermeability of the underlying silt (**Fig. 1c**), it was not included in the model.

260 Data were collected when no rain had fallen in the two preceding days. In these dry  
261 hydrological conditions, surface runoff was assumed to be negligible in the mass balance and  
262 other than the two canals discharging into the boxes, no surface water inputs were taken into  
263 consideration. Since all field measurement were completed within a few hours, evaporation of  
264 stream water and precipitation were assumed to be negligible in the mass balance. In this case,  
265 only groundwater ( $\Delta Q_{gw}$ ) and canals ( $Q_{can}$ ) composed the total water inflow downstream  
266  $\Delta Q_{downstream}$  (eq. 2) :

267 
$$\Delta Q_{downstream} = \Delta Q_{gw} + Q_{can} \quad (2)$$

268 In these conditions, the stream was assumed to be in a steady state with respect to radon.  
269 Hyporheic fluxes were also included in the groundwater flow. The estimated groundwater  
270 discharge  $\Delta Q_{gw}$  includes groundwater *sensu stricto* and hyporheic flux (Avery et al., 2018).  
271 The concentration of radon in a box was assumed to be the average concentration of radon in  
272 the inflow and the outflow (**Fig. 2**).

273 **3.6.1.2. Radon sampling and analysis**

274 Radon source and sinks used in the mass balance are summarised in **Table 3**. Next, we describe  
275 in detail the methods applied to measure radon concentrations in water, diffuse radon inputs  
276 from sediments, and atmospheric evasion.

277 Water was sampled once a month from January to July 2018 at five stations in the stream at 0,  
278 50, 700, 750, 1 850 and 2 000 m downstream from the gauging station and in the two canals  
279 (**Fig. 1c**). Groundwater was sampled during the same period at piezometers P4 and St Aunes  
280 (same sampling as section 2.5.4). Water was sampled 20 cm below the surface using an  
281 immersed pump and primed directly into 2L bottles, thereby ensuring that the water sampled

282 did not exchange any gas with the atmosphere. Conductivity of the sampled water was  
283 measured with a WTW 3620 multiparameter probe.

284 Radon in the samples was analysed using an electronic Radon-in-air monitor (Rad7, DurrIDGE  
285 Co.).  $^{222}\text{Rn}$  was extracted from the water by continuous recirculation of air in a closed loop  
286 until it reached equilibrium. Equilibrium values in air were corrected to in-water values using  
287 standard methods (Burnett and Dulaiova, 2003; Stieglitz et al., 2013) (**Table 3**).

288 In order to determine diffuse inputs of radon, sediments were sampled from the bed of the  
289 Salaison River and incubated in a 2 L bottle filled with water (average dry weight: 11.92 g,  
290  $\sigma=0.98$ ,  $n=4$ ) (Stieglitz et al., 2013). Samples were analysed with a Rad7 one month after being  
291 collected, when the sediments were assumed to be in equilibrium with the water, i.e. radon  
292 production equals radon loss by decay (Cook et al., 2008). The radon production rate can be  
293 estimated as follows (eq. 3):

294 
$$F_{diff} = C_{eq} \cdot \lambda \cdot \frac{R_{inc}}{R_{field}} \quad (3)$$

295 where  $C_{eq}$  is the concentration of radon at equilibrium ( $\text{Bq}\cdot\text{m}^{-3}$ ),  $R_{inc}$  and  $R_{field}$  are the ratios of  
296 the volume of water to that of the sediment in the incubated sample and in the field,  
297 respectively. Average sediment depth was estimated at 0.4 m based on field observations.  
298 Average radon diffusion ( $F_{diff}$ ) was calculated to be  $600 \pm 150 \text{ Bq}\cdot\text{m}^{-2}\cdot\text{d}^{-1}$  ( $n = 6$ ).

299 Khadka et al. 2017 developed a method to assess atmospheric evasion at a known water  
300 temperature, density and velocity. Using this method in our study, atmospheric evasion ( $k$ )  
301 ranged between  $1.6 \cdot 10^{-5}$  to  $2.5 \cdot 10^{-5} \text{ m}\cdot\text{s}^{-1}$  across the campaigns and was assumed to be constant  
302 in the stream for each campaign.

303 In each sampling campaign, water flow was gauged manually at the gauging station  $Q_{station}$  and  
304 in the two canals  $Q_{can}$  as water flow inputs to the mass balance (**Table 3**). In addition, water  
305 flow at the Salaison outlet was gauged manually to validate the model outputs  $\Delta Q_{downstream}$  with  
306 differential gauging.

307 To understand the link between groundwater inflow and groundwater dynamics and  
308 hydrological conditions, daily time series of water table fluctuation were obtained from the  
309 Saint Aunes piezometer on the ADES database (<http://ades.eaufrance.fr> / [ID number BSS](http://ades.eaufrance.fr)  
310 [09915X0181/AUNES](http://ades.eaufrance.fr)), and annual rainfall data from the Meteo France database (Fréjorgues  
311 weather station).

### 312 **3.6.2. DIN sampling and analysis downstream from the gauging station**

313 At the same time as water was sampled for radon analysis, water was sampled to measure the  
314 concentration of DIN in the stream, the two canals and at piezometers P4 and St Aunes as  
315 described above in section 2.6.1.2 (**Fig 1c**).

316 Water samples were taken in HDPE 100 mL bottles, previously washed with analytical grade  
317 HCl 1.2N and rinsed with ultrapure water (UW) at the laboratory. All the sampling equipment  
318 and filters were rinsed with native water before sampling. Samples were filtered through a 100  
319  $\mu\text{m}$  filter for nitrate ( $\text{NO}_3$ ), nitrite ( $\text{NO}_2$ ), ammonium ( $\text{NH}_4$ ), to prevent particles from  
320 interfering with the analysis of dissolved nutrients. Samples were immediately stored at  $-25^\circ\text{C}$

321 until analysis. The concentrations of the 3 forms of dissolved inorganic nitrogen were measured  
 322 using SEAL AA3 Analytical Autoanalyzers using the method described in Aminot and Kerouel  
 323 (2007) with colorimetric detection (from SEAL Analytical, Germany) and fluorimetric  
 324 detection (from JASCO, FP-2020plus, France) respectively for, NO<sub>2</sub>/NO<sub>3</sub> and NH<sub>4</sub>. NID  
 325 concentration was the sum of nitrites, nitrates and ammonium concentrations for each sample.  
 326 Analytical grade standards KNO<sub>3</sub>, NaNO<sub>2</sub>, (NH<sub>4</sub>)<sub>2</sub>SO<sub>4</sub> were obtained from Sigma-Aldrich (St.  
 327 Quentin Fallavier, France). Stock standard solutions were prepared in UW and stored in  
 328 waterproof HDPE bottles at room temperature in the dark at the laboratory. Fresh working  
 329 standards and calibration solutions were prepared daily by appropriate dilution of the stock  
 330 solutions using gravimetric procedures. Laboratory quality controls (QC) were performed daily  
 331 using gravimetric procedures and CertiPUR® NIST solutions (Merck, St-Quentin-en-  
 332 Yvelines, France), to validate each analysis. The linearity of the calibration curves was always  
 333 greater than R<sup>2</sup> = 0.9996. The limits of detection (LOD) were 0.05, 0.25 and 0.05 μmol.L<sup>-1</sup> for  
 334 respectively, NO<sub>2</sub>, NO<sub>3</sub> and NH<sub>4</sub>.

### 335 3.6.3. Estimation of annual DIN inputs downstream from the gauging station

336 The DIN flux at Salaison outlet was estimated as the sum of the DIN flux upstream and  
 337 downstream, assuming negligible in-stream nitrogen consumption (i.e.  $f_{station} + \Delta f_{downstream}$ ).  
 338 The increase factor  $\phi_N$  between the DIN flux at the Salaison gauging station  $f_{station}$  and the DIN  
 339 flux at the outlet was estimated as follows (eq. 4):

$$340 \phi_N = \frac{f_{station} + \Delta f_{downstream}}{f_{station}} \quad (4)$$

341 Annual increase factor I<sub>N</sub> was estimated for each hydrological year from 2013-2014 to 2017-  
 342 2018 using the frequency of each water flow class in each hydrological year.

### 343 3.6.4. Groundwater driven DIN fluxes downstream from the gauging station

344 In the downstream part of the river, assuming negligible additional surface fluxes (2.3.1), DIN  
 345 fluxes  $\Delta f_{downstream}$  were assumed to be the sum of groundwater-driven DIN fluxes  $\Delta f_{gw}$  and  
 346 canal DIN fluxes  $f_{can}$  (eq. 5):

$$347 \Delta f_{downstream} = \Delta f_{gw} + f_{can} \quad (5)$$

348 The relation between DIN and radon concentrations in the stream was used to determine the  
 349 groundwater end-member downstream [N]<sub>gw\_d</sub>.

## 350 4. Results

### 351 4.1. Groundwater catchment of the Salaison River

352 The groundwater catchment i.e. the part of the aquifer connected to the Salaison River  
353 delineated by the piezometric crest on both sides of the river covers 32.9 km<sup>2</sup>, which is 42%  
354 bigger than the Salaison watershed (i.e. surface water catchment) (**Fig. 3**). Piezometric contours  
355 show a main channel flowing from the north west to the south east of the aquifer underlying  
356 the stream, suggesting significant interactions between surface and groundwater. The contours  
357 suggest that on the most upstream part, water inflows from the stream to the aquifer, and  
358 downstream, the aquifer discharges into the stream. Along the last 4 km of the stream (i.e.  
359 where groundwater feeds the Salaison River), the hydraulic gradient decreases from 0.46 %  
360 upstream from the gauging station to 0.15 % downstream. Groundwater discharge may  
361 consequently be significant all along the downstream part of the Salaison River. Combined  
362 with the geological data, which revealed impermeable sediment units close to the lagoon, the  
363 decreasing hydraulic gradient showed that submarine discharge to the lagoon must be  
364 negligible, confirming previous conclusions.

### 365 4.2. Groundwater contribution to DIN fluxes upstream from the Salaison gauging 366 station

367 Annual DIN inputs at the gauging station ( $F_{\text{station}}$ ) ranged from  $4.5 \pm 1.8 \text{ tN.y}^{-1}$  for the dry  
368 hydrological cycle 2013-2014 to  $55.2 \pm 20.1 \text{ tN.y}^{-1}$  for the wet hydrological cycle 2014-2015  
369 (**Fig. 4**), with  $30.5 \pm 11.1 \text{ tN.y}^{-1}$  for the hydrological cycle 2017-2018. DIN inputs were linked  
370 to annual precipitation (360 mm in 2013-2014; 1176 mm in 2014-2015). Nitrate (NO<sub>3</sub>) was the  
371 main nitrogen form in the stream, with 74% to 99% of the total DIN concentrations.

372 In 2018, concentrations of DIN in the P4 well ranged around  $600 \mu\text{mol.L}^{-1}$  and reached higher  
373 values in the St Aunes piezometer (around  $800 \mu\text{mol.L}^{-1}$ ) (**Fig. 5**). Concentrations in the  
374 piezometer P4 remained in the same range in the three sampled years, suggesting that  
375 groundwater concentrations can be considered constant in the piezometer close to the Salaison  
376 River for the last five hydrological cycles. A correlation found between DIN concentrations at  
377 the station and specific conductivity (from DREAL) from 2013 to 2018, suggests that the DIN  
378 in the Salaison River originated from a high conductivity end-member (likely to be the  
379 ‘theoretical’ groundwater end-member), diluted by mixing with a low DIN/ low conductivity  
380 end-member (**Fig. 5**). The latter end-member is likely to be surface runoff water since other  
381 DIN sources are negligible (section 2.1.2). Moreover, nitrate composed 95% to 100% of the  
382 total DIN forms in P4 and St Aunes and these proportions were similar in the stream. These  
383 results suggests that the highly enriched Villafranchien aquifer constitutes the main DIN source  
384 in the river.

385 In the upstream part of the Salaison River, the non-linear correlation between DIN  
386 concentrations and conductivity suggests that DIN in the stream cannot be the result of a  
387 conservative mixing between two end-members (**Fig. 5**). Based on high DIN concentrations /  
388 high conductivity measurements in the stream, the ‘effective’ groundwater end-member DIN  
389 concentrations are twice lower than DIN concentrations measured in the groundwater. The  
390 ‘theoretical’ groundwater end-member for DIN concentration is then reduced to the ‘effective’  
391 groundwater end-member, suggesting nitrogen assimilation in the stream (i.e. from 600

392  $\mu\text{mol.L}^{-1}$  to  $300 \mu\text{mol.L}^{-1}$ ). To estimate groundwater driven DIN inputs at the gauging station,  
393 this ‘effective groundwater’ end-member was used, i.e. a DIN concentration of  $300 \pm 100$   
394  $\mu\text{mol.L}^{-1}$  was assigned to  $[\text{N}]_{\text{gw}_s}$ .

395 The annual DIN flux from groundwater at the gauging station  $F_{\text{gw}}$  derived from hydrograph  
396 separation  $Q_{\text{gw}}$  and ‘effective’ groundwater concentration  $[\text{N}]_{\text{gw}_s}$  (in eq. 1) ranged from  $3.9 \pm$   
397  $1.3 \text{ tN.y}^{-1}$  (2013-2014) to  $44.8 \pm 14.9 \text{ tN.y}^{-1}$  (2014-2015) (**Fig. 4**), with  $25.9 \pm 8.6 \text{ tN.y}^{-1}$  for  
398 2017-2018.

399 Annual groundwater contributions to instream DIN inputs ranged from 81% (2014-2015) to  
400 87% (2013-2014), and 85% in 2017-2018. Contributions were lower for wet hydrological  
401 cycles when surface runoff was more important, but annual groundwater contributions were  
402 important as groundwater is a major DIN source in the stream. Thus, significant groundwater-  
403 driven DIN fluxes are discharged upstream from the gauging station in this perennial stream.

### 404 **4.3. Interannual DIN fluxes downstream from the Salaison gauging station**

#### 405 **4.3.1. Interannual water inflow derived from the radon mass balance**

406 Radon concentrations at piezometer P4 and St Aunes were sampled at maximum and minimum  
407 table levels (from 14.5 to 16 masl at St Aunes), and ranged from  $8\ 087 \pm 178$  to  $12\ 412 \pm 232$   
408  $\text{Bq.m}^{-3}$  for P4 and  $6\ 617 \pm 327 \text{ Bq.m}^{-3}$  to  $8\ 580 \pm 215 \text{ Bq.m}^{-3}$  for St Aunes. Radon concentrations  
409 were in the same range for the two piezometers, and radon concentrations at the P4 piezometers  
410 were used as the end-member concentration in the radon mass balance for each campaign  
411 (**Table 3**).

412 Radon concentrations in the stream at the gauging station ranged from  $751 \text{ Bq.m}^{-3}$  in January  
413 to  $1\ 378 \text{ Bq.m}^{-3}$  in June, suggesting a considerable inflow of groundwater already occurring  
414 upstream from the gauging station (**Fig. 6**). Importantly, radon concentrations increased  
415 downstream from the gauging station, indicating significant groundwater influx. The increase  
416 in radon concentration is evidence for direct groundwater discharge along the stream,  
417 consistent with the geology in this section (**Fig. 3**).

418 Downstream water flow  $\Delta Q_{\text{downstream}}$  estimated from the radon mass balance ranged from  $55 \pm$   
419  $17 \text{ L.s}^{-1}$  in July to  $230 \pm 73 \text{ L.s}^{-1}$  in January (**Fig. 7**). At the Salaison outlet, confidence intervals  
420 for water flow estimated with the radon mass balance overlapped those of manual gauging,  
421 which enabled to validate the model outputs. Groundwater discharge estimated from the radon  
422 mass balance downstream from the gauging station  $\Delta Q_{\text{gw}}$  ranged from  $43 \pm 16 \text{ L.s}^{-1}$  in July to  
423  $153 \pm 53 \text{ L.s}^{-1}$  in January, and contributed between 63% in April (high flows) and 78% in July  
424 (low flows) to the total additional discharge  $\Delta Q_{\text{downstream}}$ . The radon mass balances were carried  
425 out in different hydrological conditions (from  $58 \text{ L.s}^{-1}$  to  $825 \text{ L.s}^{-1}$  at the gauging station) but  
426 the confidence interval remained in the same order of magnitude in most of the campaigns. The  
427 absolute water flow discharging downstream, with significant uncertainties, did not seem to be  
428 correlated (in a simple way) with the water table or with water flow at the gauging station  
429  $Q_{\text{station}}$ . Nevertheless, discharge downstream from the gauging station can have a significantly  
430 impact on the water flow reaching the Salaison outlet, especially in dry conditions. For example  
431 in July, downstream water discharge  $\Delta Q_{\text{downstream}}$  increased water flow at the gauging station  
432  $Q_{\text{station}}$  from  $58 \text{ L.s}^{-1}$  to  $113 \text{ L.s}^{-1}$  at the outlet.

#### 4.3.1. Annual DIN inputs downstream

The relative increase in the DIN flux between the gauging station and the outlet  $\phi_N$  was inversely correlated with the hydrological conditions (Fig. 8). When the water flow was low at the gauging station (dry conditions in July), the groundwater driven DIN flux downstream from the gauging station significantly increased the DIN flux at the Salaison outlet to a factor  $2.3 \pm 0.2$ . Conversely, in wet hydrological conditions (April), water flow at the outlet increased by a factor  $1.1 \pm 0.1$ . Absolute downstream DIN inputs remained in the same order of magnitude but, depending on the hydrological conditions, these inputs may have a significant influence on DIN flow at the outlet.

The annual increase factor  $I_N$  extrapolated from frequency-weighted water flow classes ranged from  $1.8 \pm 0.4$  in 2014-2015 (in wet conditions) to  $2.3 \pm 0.6$  in 2013-2014 (in dry conditions), and  $1.9 \pm 0.5$  in 2017-2018. Annual DIN fluxes discharged directly into the downstream part of the Salaison River  $\Delta F_{\text{downstream}}$  estimated with the annual increase factor  $I_N$  ranged from  $5.6 \pm 1.4 \text{ tN.y}^{-1}$  (2013-2014) and  $43.1 \pm 20.1 \text{ tN.y}^{-1}$  (2014-2015), and  $28.1 \pm 10.3 \text{ tN.y}^{-1}$  in 2017-2018.

#### 4.3.2. Contribution of groundwater to the interannual DIN flux downstream

On the downstream part of Salaison River, the positive correlation between DIN and radon concentrations suggests that the DIN in the stream originated from the groundwater (Fig. 9). Maximum DIN values in the stream ranged between 300 and 400  $\mu\text{mol.L}^{-1}$ , which was similar to the value used for the 'effective groundwater end-member' upstream ( $[N]_{\text{gw}_s}$ ). With the similar end-member characteristics downstream (i.e.  $[N]_{\text{gw}_d} = 300 \pm 100 \mu\text{mol.L}^{-1}$ ), the contribution of groundwater to the DIN flux downstream from the gauging station ranged from 56% in April (high flow) to 73% in July (low flows).

The concentration of radon in the Balaurie and Roubine canals ( $C_{\text{can}}$ ) ranged from 2 298 to 7 664  $\text{Bq.m}^{-3}$ , and their high radon and DIN concentrations were close to the values measured at the piezometers (Fig. 9). In addition, conductivity in the downstream part and the canals was high for all campaigns and reached the groundwater characteristics (Fig. 6). Since the field campaigns were conducted in dry periods, water discharging from these short canals probably only originate from groundwater and drain the lower aquifer units. Average flow in the Balaurie and Roubine canals remained between 20  $\text{L.s}^{-1}$  in dry hydrological conditions and 50  $\text{L.s}^{-1}$  in wet hydrological conditions. Consequently, canal discharge was counted as groundwater inflow, to be added to direct inflow to the main Salaison channel, meaning that groundwater contribution to total DIN flux in the downstream part was 100%.

#### 4.4. Overall groundwater contribution to the inputs at Salaison outlet

At the Salaison outlet, the downstream inputs from groundwater and canals significantly increased the total DIN inputs reaching Or lagoon (i.e.  $F_{\text{station}} + \Delta F_{\text{downstream}}$ ), which ranged from 10  $\text{tN.y}^{-1}$  (2013-2014) to 98  $\text{tN.y}^{-1}$  (2014-2015), with 59  $\text{tN.y}^{-1}$  in 2017-2018 (Fig. 10). The last part of the stream located in the immediate coastal environment was responsible for 44% (2014-2015) to 56% (2013-2014) of the DIN inputs to the Or lagoon, and 48% in 2017-2018.

The contribution of groundwater to annual DIN inputs at the Salaison outlet estimated with the annual groundwater-driven DIN inputs at the Salaison outlet (i.e.  $F_{\text{gw}} + \Delta F_{\text{gw}}$ ) and DIN inputs

474 at the Salaison outlet (i.e.  $F_{\text{station}} + \Delta F_{\text{downstream}}$ ) ranged from 89% (2014-2015) to 94% (2013-  
475 2014). Hence, adding the results obtained from the downstream part of the Salaison to the  
476 annual DIN inputs increased the overall contribution of groundwater to this perennial stream,  
477 making it the main source of DIN in the stream.

## 478 5. Discussion

### 479 5.1. Uncertainties on the combined methods

#### 480 5.1.1. Uncertainties on the piezometric contours

481 Piezometric contours were determined from measurements of the level of well water for one  
482 campaign in high flows (**Fig. 3**). The lack of information about aquifer geometry (cross-  
483 section) and hydrodynamic parameters (hydraulic transmissivity) did not allow to estimate  
484 groundwater flows using Darcy's law (Schilling and Wolter, 2007), but the method  
485 nevertheless provides a first qualitative overview of surface water / groundwater interactions  
486 around the Salaison River. Indeed, the hydraulic gradients estimated from the piezometric  
487 contours confirm the importance of the downstream part of the stream. Groundwater  
488 contributions to DIN inputs in the stream were estimated without using the groundwater  
489 catchment data, and adding a qualitative overview from a broader scale supports the  
490 conclusions of the study on the hydrogeological functioning of the area.

#### 491 5.1.2. Uncertainties on DIN inputs upstream from the gauging station

492 Hydrograph separation of high frequency water flow data combined with previous stream data  
493 analysis made it possible to assess the contribution of groundwater, and the baseflow results in  
494 this study are in agreement with those of a perennial stream (Eckhardt, 2008). Our results  
495 highlight the fact that, as the main source of DIN in the stream, groundwater was diluted by a  
496 low DIN / low conductivity surface water end-member (**Fig. 5**). Nevertheless, surface driven  
497 DIN fluxes can be significant even with low DIN concentrations, especially during flood events  
498 where water flow increases significantly. Thus, considering that groundwater contribution at  
499 the gauging station was 100% would have led to an overestimation of groundwater loads.

500 The non-conservative relation of DIN with conductivity upstream from the gauging station  
501 suggested that using DIN concentrations in groundwater from 'theoretical' groundwater end-  
502 member would have overestimated the DIN flux upstream from the gauging station (**Fig. 5**).  
503 The concentrations of DIN measured in the stream at the gauging station represent the  
504 combination of DIN inputs and DIN consumption upstream, either during the transit between  
505 the aquifer and the stream or during transit along the stream, for example due to uptake by  
506 plants or consumption by microorganisms (Cooper, 1990). Indeed, not taking the consumption  
507 processes along the stream into account would have led to a 50% overestimation (i.e. from the  
508 'theoretical' end-member  $600 \mu\text{mol.L}^{-1}$  to the 'effective' end-members  $300 \mu\text{mol.L}^{-1}$ ). Still,  
509 estimating the groundwater driven DIN flux with a constant 'effective' end-member  
510 concentration deduced from groundwater samples relies on the assumption that mixing with  
511 surface water is conservative. **Figure 5** shows that, in practice, this is not the case, but the  
512 'effective' groundwater end-member provides a more realistic estimation of the contribution  
513 of groundwater upstream. Additional data for DIN for conductivity between 800 and 1200  
514  $\mu\text{S.cm}^{-1}$  in the stream would enable to reduce the uncertainty of the groundwater end-member  
515 (i.e. conductivity associated with the 'effective groundwater end-member') (**Fig. 5**).

#### 516 5.1.3. Uncertainties on DIN inputs downstream from the gauging station

517 The absolute uncertainty of groundwater inflow estimated from the radon mass balance  $\Delta Q_{\text{gw}}$   
518 is related to all mass balance parameters, with higher uncertainty for the April and May  
519 campaigns (**Fig. 7**). The main parameters which influence uncertainty are the choice of radon



520 end-member concentrations and discharge measurements (as initial inputs to the model).  
521 Despite their high uncertainties, the model outputs (water flow at the Salaison outlet) are within  
522 the same confidence intervals as manual gauging at the outlet. Importantly, the results of this  
523 study suggest that all the water that discharged into the downstream part of the river was  
524 groundwater driven (direct inflow + canal inputs) (**Fig. 9**). In future studies, differential water  
525 flow gauging between the gauging station and the outlet would be sufficient to estimate the  
526 additional groundwater flow (for periods with no significant surface flow).

527 Groundwater inputs downstream from the gauging station estimated in this study were  
528 extrapolated to obtain an overall DIN flux at the scale of a hydrological cycle, based on the  
529 assumption that the 7-month campaigns were representative of the whole hydrological year.  
530 Indeed, the first months of the hydrological cycle 2017-2018 were particularly dry (**Fig. 7**),  
531 with 56 mm of rainfall from September to December 2017. Furthermore, the seven campaigns  
532 were able to capture different water flows (from 55 L.s<sup>-1</sup> to 825 L.s<sup>-1</sup>) which are representative  
533 of 92% of the hydrological conditions in the stream. Thus, studying water flow and changes in  
534 DIN flux in seven campaigns conducted from January to July enabled us to estimate the general  
535 interaction processes between the groundwater and the surface water for the whole  
536 hydrological cycle (from September to the following August), even though it is difficult to  
537 capture the correlation with the behaviour of the aquifer. Sampling campaigns did not capture  
538 flood events, but the results of this study show that the relative increase in high flows was not  
539 significant (**Fig. 8**). Indeed, water flow and DIN flux were already high at the gauging station  
540 and remained stable until the outlet.

#### 541 **5.1.4. Combining methods to understand surface water / groundwater** 542 **interaction in the Salaison River**

543 In this study, complementary methods were used to improve our understanding of surface water  
544 / groundwater interactions along the Salaison River. High frequency water flow and DIN data  
545 were available for the upstream part of the Salaison, enabling the use of hydrograph baseflow  
546 separation and flow interval classification methods to estimate DIN fluxes. Downstream from  
547 the gauging station, a radon mass balance highlighted the predominance of groundwater driven  
548 DIN inputs in this part of the stream. Combining the results of the downstream radon mass  
549 balance with results of the upstream hydrograph separation results enabled estimation of  
550 groundwater-driven DIN fluxes at the Salaison outlet. Combining the methods did not reduce  
551 uncertainties, but validated the robustness of the results by approaching the study from different  
552 angles (Baudron et al., 2015; Martinez et al., 2015).

#### 553 **5.2. Importance of the downstream part of the Salaison River**

554 This study demonstrated that the majority of DIN fluxes at the Salaison River outlet are  
555 groundwater driven (**Fig. 10**). As a perennial stream, groundwater is a major contributor to  
556 stream flow and an even more important contributor to DIN as a result of the high DIN  
557 concentrations in the aquifer (Adyasari et al., 2018; Exner-Kittridge et al., 2016; Schilling et  
558 al., 2018). The downstream part of the Salaison River in particular delivers 44% to 56% of the  
559 DIN inputs to the Or lagoon, even though it only covers 25% of the surface watershed.  
560 Moreover, inputs of groundwater downstream are less likely to be consumed before arriving at

561 the Salaison outlet compared with inputs to the upstream part of the stream, since their transit  
562 time before reaching the outlet is shorter (Seitzinger, 1988).

563 In addition, the water in the two canals located downstream from the gauging station originates  
564 from groundwater (**Fig. 9**). The original purpose of the two canals was to receive waste water  
565 and storm water in high flow conditions (Aquascop, 2013), but they also acted as pathways  
566 which enabled groundwater to reach the main channel by improving its drainage contact with  
567 the aquifer (Rozemeijer and Broers, 2007). Groundwater is carried to the Salaison river through  
568 these outlets, adding flow to the direct groundwater discharge which occurs all along the river.  
569 The Roubine canal delivers a significant proportion of the groundwater flow (from 10 to 40  
570  $L.s^{-1}$ ) to the last part of the Salaison River and the short transit time before reaching Or lagoon  
571 limits the consumption of associated DIN fluxes.

572 Inflows of groundwater to the downstream part of the Salaison River are a major source of DIN  
573 and these inputs are not monitored by the gauging station, suggesting that the position of the  
574 gauging station may have a significant impact on the estimation of DIN fluxes at the Salaison  
575 outlet (**Fig. 10**). Locating the Salaison gauging station 2 000 m downstream, at the limit  
576 between alluvial bedrock and lagoon silt would make it possible to monitor water flow and  
577 DIN concentrations more accurately while still avoiding the intrusion of lagoon water (**Fig. 3**).  
578 The results of this study emphasize the need to understand surface water /groundwater  
579 interactions on the continent to satisfactorily monitor nutrient fluxes to the coastal zone  
580 (Delconte et al., 2014; Jin et al., 2016). Nevertheless, for the five hydrological cycles studied,  
581 annual DIN inputs at the Salaison outlet were found to be correlated with annual rainfall  
582 ( $R^2=0.92$ ;  $y = 0.106x - 26$ , *data not shown*). Thus, available rainfall data could provide a  
583 preliminary estimation of the annual load reaching the Or lagoon, as long as groundwater and  
584 surface runoff constitute the main DIN sources in the stream.

### 585 **5.3. Groundwater is a significant source of DIN in the Or lagoon**

586 The final aim of this study was to estimate total DIN inputs from the alluvial aquifer to the Or  
587 lagoon. Previous studies had concluded that no direct submarine groundwater discharge in the  
588 lagoon or from other groundwater pathways from the Villafranchien aquifer to the Or lagoon  
589 needed to be identified. Since geological characteristics on the northern border of the lagoon  
590 at the limit with the aquifer are similar for all the northern streams, our work focused on the  
591 Salaison River as a representative area for surface water / groundwater interactions. First, the  
592 hydraulic gradients from the piezometric contour of the aquifer around the Salaison river  
593 indicated that in high flow conditions, most of the groundwater discharges upstream from the  
594 silt layer (**Fig. 3**). A change in permeability must cause groundwater outflow upstream from  
595 the alluvium/silt interface (Santamaria, 1995), not only in the Salaison groundwater catchment  
596 but also in the surrounding wetlands on the northern part of the lagoon (**Fig. 1a**). In these areas,  
597 evaporation and plant uptake are high and man-made embankments often divide up the natural  
598 areas, so the real quantity of water that arrives in the lagoon in this way may be negligible. The  
599 streams thus represent the only outlets for the water table, with the Salaison River as one of the  
600 main streams. Although the Salaison only accounts for 17% of the Or surface watershed, it  
601 delivers 59% of total freshwater originating from the northern streams (Colin et al., 2017) and,  
602 according to our results, including significant groundwater-driven inputs of DIN (> 90%) (**Fig.**

603 **10).** This study demonstrates that the Salaison River is a major conveyor of groundwater-driven  
604 DIN to the Or lagoon, and is probably representative of groundwater inputs to the Or lagoon  
605 from other natural streams nearby, owing to similar hydrology and hydrogeology. Moreover,  
606 the important aquifer interaction with the stream could explain the important contribution of  
607 the Salaison to the freshwater inputs in comparison with its small watershed.

608 To estimate groundwater driven DIN inputs from all these northern streams, two extreme  
609 hydrological behaviours can be assumed. First, the Salaison can be considered as the only  
610 stream fed by groundwater in the northern part of the watershed. Hence, depending on  
611 hydrological conditions, this study suggests that 10 (dry hydrological cycle) to 98 tN.y<sup>-1</sup> (wet  
612 hydrological cycle) originating from the Villafranchien aquifer reach the Or lagoon every year  
613 (**Fig. 10**). It can also be assumed that all the northern streams are characterised by similar  
614 surface water/groundwater interactions and DIN end-members as those of the Salaison River.  
615 Since these stream supply 40% of freshwater to the Or lagoon (Colin et al., 2017), assuming  
616 that 90% of this freshwater originates from groundwater, DIN inputs can be estimated. In this  
617 case, 17 (dry hydrological cycle) to 163 tN.y<sup>-1</sup> (wet hydrological cycle) of groundwater driven  
618 DIN reach the Or lagoon. Extrapolations to other northern streams involve considerable  
619 uncertainties because (1) the surface water in other parts of the aquifer might constitute a  
620 significant DIN source depending on land occupation, (2) the groundwater catchment of the  
621 Salaison River is larger than the surface watershed, thereby reducing the aquifer system of  
622 other streams including their groundwater discharge (**Fig. 3**). Despite these uncertainties, these  
623 simple estimations provide an order of magnitude for total groundwater driven DIN inputs to  
624 the Or lagoon, with minimum (results for the Salaison only) and maximum values.

#### 625 **5.4. Implications for managements actions in the Or lagoon**

626 This study has shown that, even though groundwater does not discharge directly into the  
627 lagoon, groundwater-driven inputs to the inflowing stream are a significant source of DIN to  
628 the Or lagoon and are only partially taken into account in current observations made at the  
629 gauging stations. Our investigation focussed on DIN, at the origin of eutrophication - with the  
630 predominance of nitrate from the Salaison (74% to 99% of total DIN). Similar considerations  
631 apply to phosphorus or crop protection products (pesticides), for example, and, depending on  
632 concentration in the groundwater and the half-life of the molecule concerned, inputs to the  
633 coast may also be significant. This study has shown that the aquifer and its subsurface  
634 catchment have to be taken into account in territorial strategies (Adyasari et al., 2018; Stieglitz  
635 et al., 2013). This implies that the area targeted by management actions aimed at reducing  
636 inputs of the nutrient to the coastal zone has to extend from the watershed to the groundwater  
637 catchment. The residence time of water in the aquifer is another important parameter to take  
638 into account in management planning and monitoring: if the travel time is long, results of  
639 management actions will only be observed with a significant lag time (Fenton et al., 2011; van  
640 Lanen and Dijkma, 1999; Vervloet et al., 2018). Concentrations of DIN in the aquifer have  
641 remained relatively constant in the past decade, evidence that management actions in the  
642 watershed have not improved the quality of the groundwater so far. Groundwater dating should  
643 give an indication of time needed to see improvement in the nutrient concentration at the  
644 aquifer outlet (Aquilina et al., 2012).

645 **Conclusions**

646 The complementary methods used in this study enabled us to investigate surface water /  
647 groundwater interactions in the upstream and downstream sections of the Salaison River.  
648 Groundwater was shown to be the main source of DIN (mainly NO<sub>3</sub>) contamination of the  
649 Salaison River, thereby revealing streams to be indirect pathways for groundwater to reach the  
650 Or lagoon. Inputs are naturally governed by hydrogeological conditions and are usually  
651 considerably underestimated when they are only measured at the gauging station. The high  
652 level of groundwater driven DIN inputs estimated in this study could inhibit restoration of the  
653 Or lagoon for many years. The results of the study improve our understanding of indirect  
654 groundwater-driven nutrient inputs from an alluvial aquifer to the coastal zone and of the  
655 land/sea continuum.

656 **Acknowledgements**

657 This research was funded by the French National Research Agency (ANR) through the ANR  
658 @RAction chair of excellence (ANR-14-ACHN-0007-01 - T Stieglitz). This research is part  
659 of a PhD projet funded by IFREMER, BRGM and CEREGE. The authors acknowledge A  
660 Nefzi, E Bousquet and S Pistre for their support with data collection and analysis. We are  
661 grateful to F Maldan (BRGM Montpellier) for all his help in the field, and also to C Saguet and  
662 L Dijoux (IFREMER Sète). DIN samples were analysed at IFREMER Sète laboratory  
663 (COFRAC - accredited) with the help of M Fortune, E Foucault and G Messiaen. We thank F  
664 Colin (SupAgro Montpellier), R De Wit (CNRS Montpellier), E Roque (IFREMER Sète), P  
665 Souchu (IFREMER Nantes) and JB Martin (University of Florida) for constructive comments  
666 on our paper. We are grateful of the two reviewers that provided useful comments to improve  
667 the manuscript.

668 **References**

- 669 Adyasari, D., Oehler, T., Afiati, N., Moosdorf, N., 2018. Groundwater nutrient inputs into an  
670 urbanized tropical estuary system in Indonesia. *Sci. Total Environ.* 627, 1066–1079.  
671 <https://doi.org/10.1016/J.SCITOTENV.2018.01.281>
- 672 Aminot, A., Kerouel, R., 2007. Dosage automatique des nutriments dans les eaux marines :  
673 méthodes en flux continu. Editions Ifremer, 188 p.
- 674 Aquascop, 2013. Suivi 2012 de la qualité des eaux des bassins versants de l'étang de Thau, de  
675 l'étang de l'Or, du Lez et de la Mosson. Aquascop/7197 - 307 p.
- 676 Aquilina, L., Vergnaud-Ayraud, V., Labasque, T., Bour, O., Molénat, J., Ruiz, L., de Montety,  
677 V., De Ridder, J., Roques, C., Longuevergne, L., 2012. Nitrate dynamics in agricultural  
678 catchments deduced from groundwater dating and long-term nitrate monitoring in  
679 surface- and groundwaters. *Sci. Total Environ.* 435–436, 167–178.  
680 <https://doi.org/10.1016/J.SCITOTENV.2012.06.028>
- 681 Avery, E., Bibby, R., Visser, A., Esser, B., Moran, J., 2018. Quantification of Groundwater  
682 Discharge in a Subalpine Stream Using Radon-222. *Water* 10, 100 p.  
683 <https://doi.org/10.3390/w10020100>
- 684 Banks, E.W., Simmons, C.T., Love, A.J., Shand, P., 2011. Assessing spatial and temporal  
685 connectivity between surface water and groundwater in a regional catchment:  
686 Implications for regional scale water quantity and quality. *J. Hydrol.* 404, 30–49.  
687 <https://doi.org/10.1016/J.JHYDROL.2011.04.017>
- 688 Basset, A., Elliott, M., West, R.J., Wilson, J.G., 2013. Estuarine and lagoon biodiversity and  
689 their natural goods and services. *Estuar. Coast. Shelf Sci.* 132, 1–4.  
690 <https://doi.org/10.1016/J.ECSS.2013.05.018>
- 691 Baudron, P., Cockenpot, S., Lopez-Castejon, F., Radakovitch, O., Gilabert, J., Mayer, A.,  
692 Garcia-Arostegui, J.L., Martinez-Vicente, D., Leduc, C., Claude, C., 2015. Combining  
693 radon, short-lived radium isotopes and hydrodynamic modeling to assess submarine  
694 groundwater discharge from an anthropized semiarid watershed to a Mediterranean  
695 lagoon (Mar Menor, SE Spain). *J. Hydrol.* 525, 55–71.  
696 <https://doi.org/10.1016/j.jhydrol.2015.03.015>
- 697 Blaise, M., Dorfliger, N., Le Strat, P., Ladouche, B., 2008. Etang de l'Or : relations entre les  
698 eaux souterraines de l'aquifère de sub-surface et l'étang de l'Or en liaison avec  
699 l'occupation du sol. BRGM/RP-55367-FR - 275 p.
- 700 Burnett, W.C., Aggarwal, P.K.K., Aureli, A., Bokuniewicz, H., Cable, J.E.E., Charette,  
701 M.A.A., Kontar, E., Krupa, S., Kulkarni, K.M.M., Loveless, A., Moore, W.S.S.,  
702 Oberdorfer, J.A.A., Oliveira, J., Ozyurt, N., Povinec, P., Privitera, A.M.G.M.G., Rajar,  
703 R., Ramessur, R.T.T., Scholten, J., Stieglitz, T., Taniguchi, M., Turner, J.V. V., 2006.  
704 Quantifying submarine groundwater discharge in the coastal zone via multiple methods.  
705 *Sci. Total Environ.* 367, 498–543. <https://doi.org/10.1016/j.scitotenv.2006.05.009>

- 706 Burnett, W.C., Dulaiova, H., 2003. Estimating the dynamics of groundwater input into the  
707 coastal zone via continuous radon-222 measurements. *J. Environ. Radioact.* 69, 21–35.  
708 [https://doi.org/10.1016/S0265-931X\(03\)00084-5](https://doi.org/10.1016/S0265-931X(03)00084-5)
- 709 Burnett, W.C., Taniguchi, M., Oberdorfer, J., 2001. Measurement and significance of the direct  
710 discharge of groundwater into the coastal zone. *J. Sea Res.* 46, 109–116.  
711 [https://doi.org/10.1016/S1385-1101\(01\)00075-2](https://doi.org/10.1016/S1385-1101(01)00075-2)
- 712 Chapman, T., 1999. A comparison of algorithms for stream flow recession and baseflow  
713 separation. *Hydrol. Process.* 13, 701–714. [https://doi.org/10.1002/\(SICI\)1099-  
714 1085\(19990415\)13:5<701::AID-HYP774>3.0.CO;2-2](https://doi.org/10.1002/(SICI)1099-1085(19990415)13:5<701::AID-HYP774>3.0.CO;2-2)
- 715 Charette, M.A., Buesseler, K.O., Andrews, J.E., 2001. Utility of radium isotopes for evaluating  
716 the input and transport of groundwater-derived nitrogen to a Cape Cod estuary. *Limnol.*  
717 *Oceanogr.* 46, 465–470. <https://doi.org/10.4319/lo.2001.46.2.0465>
- 718 Cloern, J.E., 2001. Our evolving conceptual model of the coastal eutrophication problem. *Mar.*  
719 *Ecol. Prog. Ser.* <https://doi.org/10.3354/meps210223>
- 720 Colin, F., Crabit, A., Augas, J., Garnier, F., Favre, L., Lilti, V., Verlingue, U., 2017. Apports  
721 d'eau aux lagunes côtières méditerranéennes - Propositions méthodologiques pour la  
722 quantification des écoulements basées sur des mesures légères et des modèles  
723 synthétiques. Rapport de fin de projet Agence de l'Eau RMC. Montpellier SupAgro - 50  
724 p.
- 725 Cook, P.G., Favreau, G., Dighton, J.C., Tickell, S., 2003. Determining natural groundwater  
726 influx to a tropical river using radon, chlorofluorocarbons and ionic environmental tracers.  
727 *J. Hydrol.* 277, 74–88. [https://doi.org/10.1016/S0022-1694\(03\)00087-8](https://doi.org/10.1016/S0022-1694(03)00087-8)
- 728 Cook, P.G., Lamontagne, S., Berhane, D., Clark, J.F., 2006. Quantifying groundwater  
729 discharge to Cockburn River, southeastern Australia, using dissolved gas tracers <sup>222</sup>Rn  
730 and SF<sub>6</sub>. *Water Resour. Res.* 42. <https://doi.org/10.1029/2006WR004921>
- 731 Cook, P.G., Wood, C., White, T., Simmons, C.T., Fass, T., Brunner, P., 2008. Groundwater  
732 inflow to a shallow, poorly-mixed wetland estimated from a mass balance of radon. *J.*  
733 *Hydrol.* 354, 213–226. <https://doi.org/10.1016/j.jhydrol.2008.03.016>
- 734 Cooper, A.B., 1990. Nitrate depletion in the riparian zone and stream channel of a small  
735 headwater catchment. *Hydrobiologia* 202, 13–26. <https://doi.org/10.1007/BF00027089>
- 736 de Jonge, V.N., Elliott, M., Orive, E., 2002. Causes, historical development, effects and future  
737 challenges of a common environmental problem: eutrophication. *Hydrobiologia* 475/476,  
738 1–19. <https://doi.org/10.1023/A:1020366418295>
- 739 Delconte, C.A., Sacchi, E., Racchetti, E., Bartoli, M., Mas-Pla, J., Re, V., 2014. Nitrogen inputs  
740 to a river course in a heavily impacted watershed: A combined hydrochemical and isotopic  
741 evaluation (Oglio River Basin, N Italy). *Sci. Total Environ.* 466–467, 924–938.  
742 <https://doi.org/10.1016/J.SCITOTENV.2013.07.092>
- 743 Derolez, V., Fiandrino, A., Munaron, D., 2014. Bilan sur les principales pressions pesant sur

- 744 les lagunes méditerranéennes et leurs liens avec l'état DCE. Rapport Ifremer/RST-  
745 LER/LR 14-20 - 46 p.
- 746 Derolez, V., Gimard, A., Munaron, D., Ouisse, V., Messiaen, G., Fortune, M., Poirrier, S.,  
747 Mortreux, S., Guillou, J.-L., Brun, M., Provost, C., Hatey, E., Bec, B., Malet, N.,  
748 Fiandrino, A., 2017. OBSLAG 2016 - volet eutrophisation. Etat DCE des lagunes  
749 méditerranéennes (eau et phytoplancton, période 2011-2016). Développement  
750 d'indicateurs de tendance et de variabilité. Ifremer/RST/LER/LR/17.10 - 75 p.
- 751 Eckhardt, K., 2008. A comparison of baseflow indices, which were calculated with seven  
752 different baseflow separation methods. *J. Hydrol.* 352, 168–173.  
753 <https://doi.org/10.1016/j.jhydrol.2008.01.005>
- 754 Eckhardt, K., 2005. How to construct recursive digital filters for baseflow separation. *Hydrol.*  
755 *Process.* 19, 507–515. <https://doi.org/10.1002/hyp.5675>
- 756 Exner-Kittridge, M., Strauss, P., Blöschl, G., Eder, A., Saracevic, E., Zessner, M., 2016. The  
757 seasonal dynamics of the stream sources and input flow paths of water and nitrogen of an  
758 Austrian headwater agricultural catchment. *Sci. Total Environ.* 542, 935–945.  
759 <https://doi.org/10.1016/J.SCITOTENV.2015.10.151>
- 760 Fenton, O., Schulte, R.P.O., Jordan, P., Lalor, S.T.J., Richards, K.G., 2011. Time lag: a  
761 methodology for the estimation of vertical and horizontal travel and flushing timescales  
762 to nitrate threshold concentrations in Irish aquifers. *Environ. Sci. Policy* 14, 419–431.  
763 <https://doi.org/10.1016/J.ENVSCI.2011.03.006>
- 764 Jin, L., Whitehead, P.G., Heppell, C.M., Lansdown, K., Purdie, D.A., Trimmer, M., 2016.  
765 Modelling flow and inorganic nitrogen dynamics on the Hampshire Avon: Linking  
766 upstream processes to downstream water quality. *Sci. Total Environ.* 572, 1496–1506.  
767 <https://doi.org/10.1016/J.SCITOTENV.2016.02.156>
- 768 Johannes, R., 1980. The Ecological Significance of the Submarine Discharge of Groundwater.  
769 *Mar. Ecol. Prog. Ser.* 3, 365–373. <https://doi.org/10.3354/meps003365>
- 770 Khadka, M.B., Martin, J.B., Kurz, M.J., 2017. Synoptic estimates of diffuse groundwater  
771 seepage to a spring-fed karst river at high spatial resolution using an automated radon  
772 measurement technique. *J. Hydrol.* 544, 86–96.  
773 <https://doi.org/10.1016/J.JHYDROL.2016.11.013>
- 774 Kjerfve, B., Magill, K., 1989. Geographic and hydrodynamic characteristics of shallow coastal  
775 lagoons. *Mar. Geol.* 88, 187–199. [https://doi.org/10.1016/0025-3227\(89\)90097-2](https://doi.org/10.1016/0025-3227(89)90097-2)
- 776 Lanini, S., Caballero, Y., Seguin, J.-J., Maréchal, J.-C., 2016. ESPERE-A Multiple-Method  
777 Microsoft Excel Application for Estimating Aquifer Recharge. *Groundwater* 54, 155–156.  
778 <https://doi.org/10.1111/gwat.12390>
- 779 Martinez, J.L., Raiber, M., Cox, M.E., 2015. Assessment of groundwater–surface water  
780 interaction using long-term hydrochemical data and isotope hydrology: Headwaters of the  
781 Condamine River, Southeast Queensland, Australia. *Sci. Total Environ.* 536, 499–516.

- 782 <https://doi.org/10.1016/J.SCITOTENV.2015.07.031>
- 783 Meinesz, C., Derolez, V., Bouchoucha, M., 2013. Base de données « pressions sur les lagunes  
784 méditerranéennes ». Analyse des liens état – pression, Rapport Ifremer RST.ODE/LER-  
785 PAC/13-11 - 71 p.
- 786 Menció, A., Galán, M., Boix, D., Mas-Pla, J., 2014. Analysis of stream–aquifer relationships:  
787 A comparison between mass balance and Darcy’s law approaches. *J. Hydrol.* 517, 157–  
788 172. <https://doi.org/10.1016/J.JHYDROL.2014.05.039>
- 789 Mooney, H., Larigauderie, A., Cesario, M., Elmquist, T., Hoegh-Guldberg, O., Lavorel, S.,  
790 Mace, G.M., Palmer, M., Scholes, R., Yahara, T., 2009. Biodiversity, climate change, and  
791 ecosystem services. *Curr. Opin. Environ. Sustain.* 1, 46–54.  
792 <https://doi.org/10.1016/J.COSUST.2009.07.006>
- 793 Moore, W.S., 2010. The Effect of Submarine Groundwater Discharge on the Ocean. *Ann. Rev.*  
794 *Mar. Sci.* 2, 59–88. <https://doi.org/10.1146/annurev-marine-120308-081019>
- 795 Mullinger, N.J., Binley, A.M., Pates, J.M., Crook, N.P., 2007. Radon in Chalk streams: Spatial  
796 and temporal variation of groundwater sources in the Pang and Lambourn catchments,  
797 UK. *J. Hydrol.* 339, 172–182. <https://doi.org/10.1016/J.JHYDROL.2007.03.010>
- 798 Newton, A., Brito, A.C., Icely, J.D., Derolez, V., Clara, I., Angus, S., Schernewski, G., Inácio,  
799 M., Lillebø, A.I., Sousa, A.I., Béjaoui, B., Solidoro, C., Tosic, M., Cañedo-Argüelles, M.,  
800 Yamamuro, M., Reizopoulou, S., Tseng, H.-C., Canu, D., Roselli, L., Maanan, M.,  
801 Cristina, S., Ruiz-Fernández, A.C., Lima, R.F. de, Kjerfve, B., Rubio-Cisneros, N., Pérez-  
802 Ruzafa, A., Marcos, C., Pastres, R., Pranovi, F., Snoussi, M., Turpie, J., Tuchkovenko,  
803 Y., Dyack, B., Brookes, J., Povilanskas, R., Khokhlov, V., 2018. Assessing, quantifying  
804 and valuing the ecosystem services of coastal lagoons. *J. Nat. Conserv.* 44, 50–65.  
805 <https://doi.org/10.1016/J.JNC.2018.02.009>
- 806 Newton, A., Icely, J., Cristina, S., Brito, A., Cardoso, A.C., Colijn, F., Riva, S.D., Gertz, F.,  
807 Hansen, J.W., Holmer, M., Ivanova, K., Leppäkoski, E., Canu, D.M., Mocenni, C.,  
808 Mudge, S., Murray, N., Pejrup, M., Razinkovas, A., Reizopoulou, S., Pérez-Ruzafa, A.,  
809 Schernewski, G., Schubert, H., Carr, L., Solidoro, C., PierluigiViaroli, Zaldívar, J.-M.,  
810 2014. An overview of ecological status, vulnerability and future perspectives of European  
811 large shallow, semi-enclosed coastal systems, lagoons and transitional waters. *Estuar.*  
812 *Coast. Shelf Sci.* 140, 95–122. <https://doi.org/10.1016/J.ECSS.2013.05.023>
- 813 Peterson, R.N., Santos, I.R., Burnett, W.C., 2010. Evaluating groundwater discharge to tidal  
814 rivers based on a Rn-222 time-series approach. *Estuar. Coast. Shelf Sci.* 86, 165–178.  
815 <https://doi.org/10.1016/J.ECSS.2009.10.022>
- 816 Quintana, X.D., Moreno-Amich, R., Comín, F.A., 1998. Nutrient and plankton dynamics in a  
817 Mediterranean salt marsh dominated by incidents of flooding. Part 1: Differential  
818 confinement of nutrients. *J. Plankton Res.* 20, 2089–2107.  
819 <https://doi.org/10.1093/plankt/20.11.2089>
- 820 Rimmelin, P., Dumon, J.-C., Maneux, E., Gonçalves, A., 1998. Study of Annual and Seasonal



- 821 Dissolved Inorganic Nitrogen Inputs into the Arcachon Lagoon, Atlantic Coast (France).  
822 Estuar. Coast. Shelf Sci. 47, 649–659. <https://doi.org/10.1006/ECSS.1998.0384>
- 823 Rodellas, V., Garcia-Orellana, J., Masqué, P., Feldman, M., Weinstein, Y., 2015. Submarine  
824 groundwater discharge as a major source of nutrients to the Mediterranean Sea. Proc. Natl.  
825 Acad. Sci. U. S. A. 112, 3926–30. <https://doi.org/10.1073/pnas.1419049112>
- 826 Rodellas, V., Stieglitz, T.C., Andrisoa, A., Cook, P.G., Raimbault, P., Tamborski, J.J., van  
827 Beek, P., Radakovitch, O., 2018. Groundwater-driven nutrient inputs to coastal lagoons:  
828 The relevance of lagoon water recirculation as a conveyor of dissolved nutrients. Sci.  
829 Total Environ. 642, 764–780. <https://doi.org/10.1016/J.SCITOTENV.2018.06.095>
- 830 Rozemeijer, J.C., Broers, H.P., 2007. The groundwater contribution to surface water  
831 contamination in a region with intensive agricultural land use (Noord-Brabant, The  
832 Netherlands). Environ. Pollut. 148, 695–706.  
833 <https://doi.org/10.1016/J.ENVPOL.2007.01.028>
- 834 Santamaria, L., 1995. Etude préliminaire des transferts d'eau et de solutés à l'étang de l'Or, au  
835 travers des formations villafranchiennes dans la plaine de Mauguio-Lunel, interface  
836 nappe-étang. Université Montpellier II/ Mémoire de fin d'études - 46 p.
- 837 Santos, I.R., Peterson, R.N., Eyre, B.D., Burnett, W.C., 2010. Significant lateral inputs of fresh  
838 groundwater into a stratified tropical estuary: Evidence from radon and radium isotopes.  
839 Mar. Chem. 121, 37–48. <https://doi.org/10.1016/J.MARCHEM.2010.03.003>
- 840 Schilling, K.E., Streeter, M.T., Bettis, E.A., Wilson, C.G., Papanicolaou, A.N., 2018.  
841 Groundwater monitoring at the watershed scale: An evaluation of recharge and nonpoint  
842 source pollutant loading in the Clear Creek Watershed, Iowa. Hydrol. Process. 32, 562–  
843 575. <https://doi.org/10.1002/hyp.11440>
- 844 Schilling, K.E., Wolter, C.F., 2007. A GIS-based groundwater travel time model to evaluate  
845 stream nitrate concentration reductions from land use change. Environ. Geol. 53, 433–  
846 443. <https://doi.org/10.1007/s00254-007-0659-0>
- 847 Schilling, K.E., Wolter, C.F., 2001. Contribution of Base Flow to Nonpoint Source Pollution  
848 Loads in an Agricultural Watershed. Ground Water 39, 49–58.  
849 <https://doi.org/10.1111/j.1745-6584.2001.tb00350.x>
- 850 Seitzinger, S.P., 1988. Denitrification in freshwater and coastal marine ecosystems: Ecological  
851 and geochemical significance. Limnol. Oceanogr. 33, 702–724.  
852 <https://doi.org/10.4319/lo.1988.33.4part2.0702>
- 853 Slomp, C.P., Van Cappellen, P., 2004. Nutrient inputs to the coastal ocean through submarine  
854 groundwater discharge: controls and potential impact. J. Hydrol. 295, 64–86.  
855 <https://doi.org/10.1016/j.jhydrol.2004.02.018>
- 856 Souchu, P., Bec, B., Smith, V.H., Laugier, T., Fiandrino, A., Benau, L., Orsoni, V., Collos, Y.,  
857 Vaquer, A., 2010. Patterns in nutrient limitation and chlorophyll a along an anthropogenic  
858 eutrophication gradient in French Mediterranean coastal lagoons. Can. J. Fish. Aquat. Sci.

859 67, 743–753. <https://doi.org/10.1139/F10-018>

860 Stieglitz, T.C., van Beek, P., Souhaut, M., Cook, P.G., 2013. Karstic groundwater discharge  
861 and seawater recirculation through sediments in shallow coastal Mediterranean lagoons,  
862 determined from water, salt and radon budgets. *Mar. Chem.* 156, 73–84.  
863 <https://doi.org/10.1016/j.marchem.2013.05.005>

864 Symbo, 2017. Tableau de bord de suivi environnemental du contrat de bassin de l’Or. OUTIL  
865 TECHNIQUE TBSE – Or 2017 - 33 p.

866 Symbo, 2014. Le Salaision, état des lieux et programme pluriannuel de gestion et de  
867 restauration. 30 p.

868 Taylor, D., Nixon, S., Granger, S., Buckley, B., 1995. Nutrient limitation and the  
869 eutrophication of coastal lagoons. *Mar. Ecol. Prog. Ser.* 127, 235–244.  
870 <https://doi.org/10.3354/meps127235>

871 van Lanen, H.A.J., Dijkma, R., 1999. Water flow and nitrate transport to a groundwater-fed  
872 stream in the Belgian-Dutch chalk region. *Hydrol. Process.* 13, 295–307.  
873 [https://doi.org/10.1002/\(SICI\)1099-1085\(19990228\)13:3<295::AID-HYP739>3.0.CO;2-](https://doi.org/10.1002/(SICI)1099-1085(19990228)13:3<295::AID-HYP739>3.0.CO;2-)  
874 O

875 Vervloet, L.S.C., Binning, P.J., Børgesen, C.D., Højberg, A.L., 2018. Delay in catchment  
876 nitrogen load to streams following restrictions on fertilizer application. *Sci. Total Environ.*  
877 627, 1154–1166. <https://doi.org/10.1016/J.SCITOTENV.2018.01.255>

878

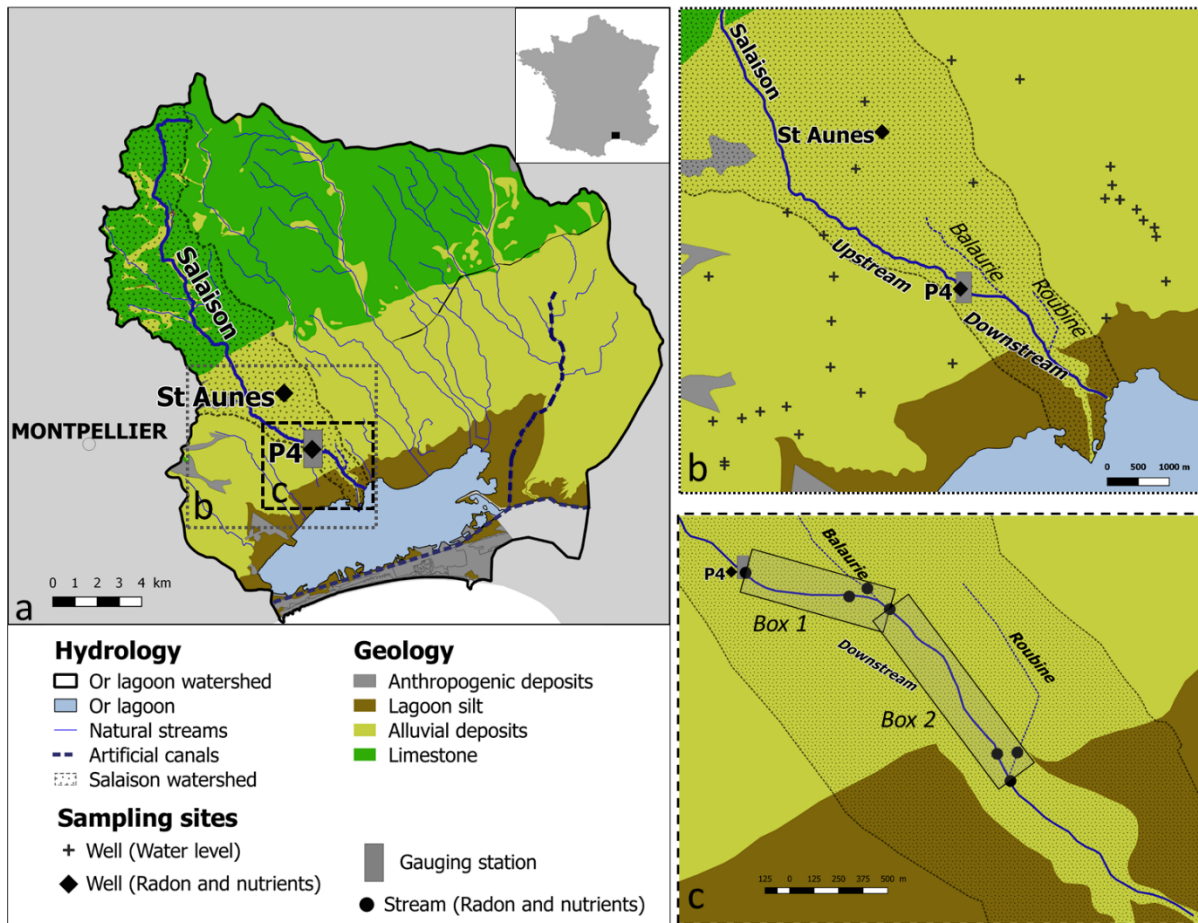


**Figure 1:** a) Hydrogeological settings and localisation of piezometers for the study site; b) Sampling stations for the piezometric map (water levelled wells) and localisation of the gauging station in Salaison river; c) Sampling sites for the radon sampling downstream of the gauging station and the two associated box models for the radon mass balance.

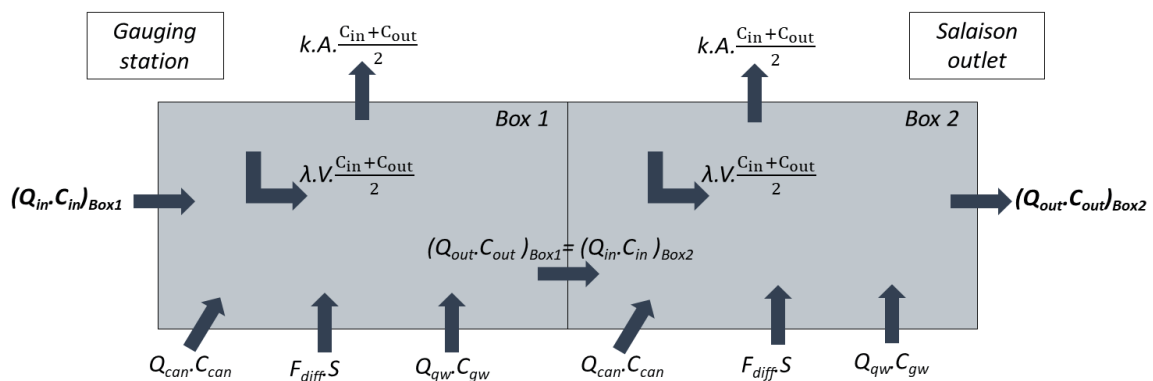


**Figure 2:** Conceptual scheme of the connected boxes for the radon mass balance in the downstream part of Salaison River: sinks and sources of radon flux ( $Bq \cdot s^{-1}$ )

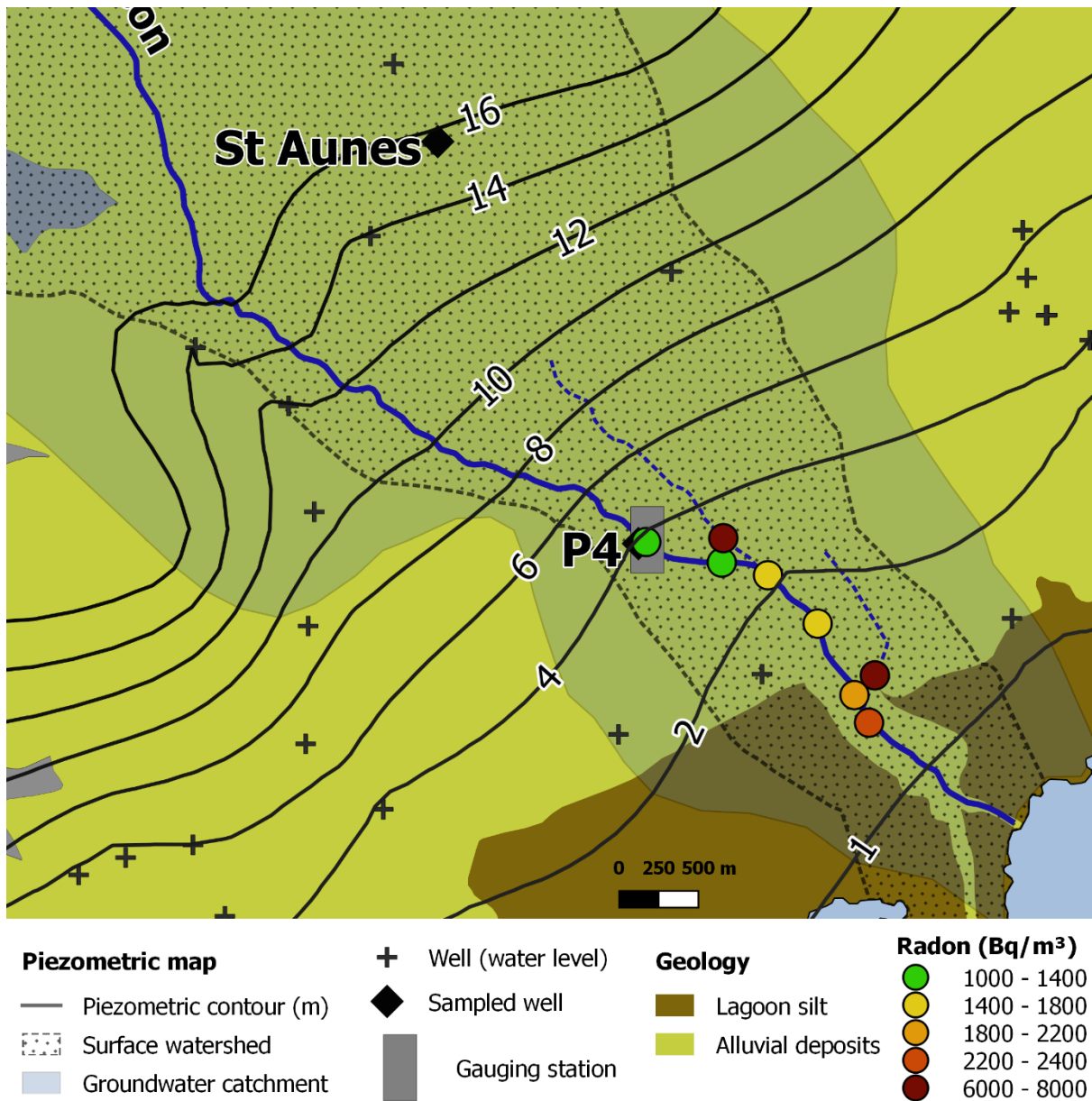


**Figure 3:** Piezometric maps describing Salaison's groundwater catchment. Salaison watershed is displayed for comparison with the groundwater catchment. On the downstream part of Salaison River, an example of radon concentrations measured on 2/15/2018 is presented, showing significant radon increase due to significant groundwater input downstream.

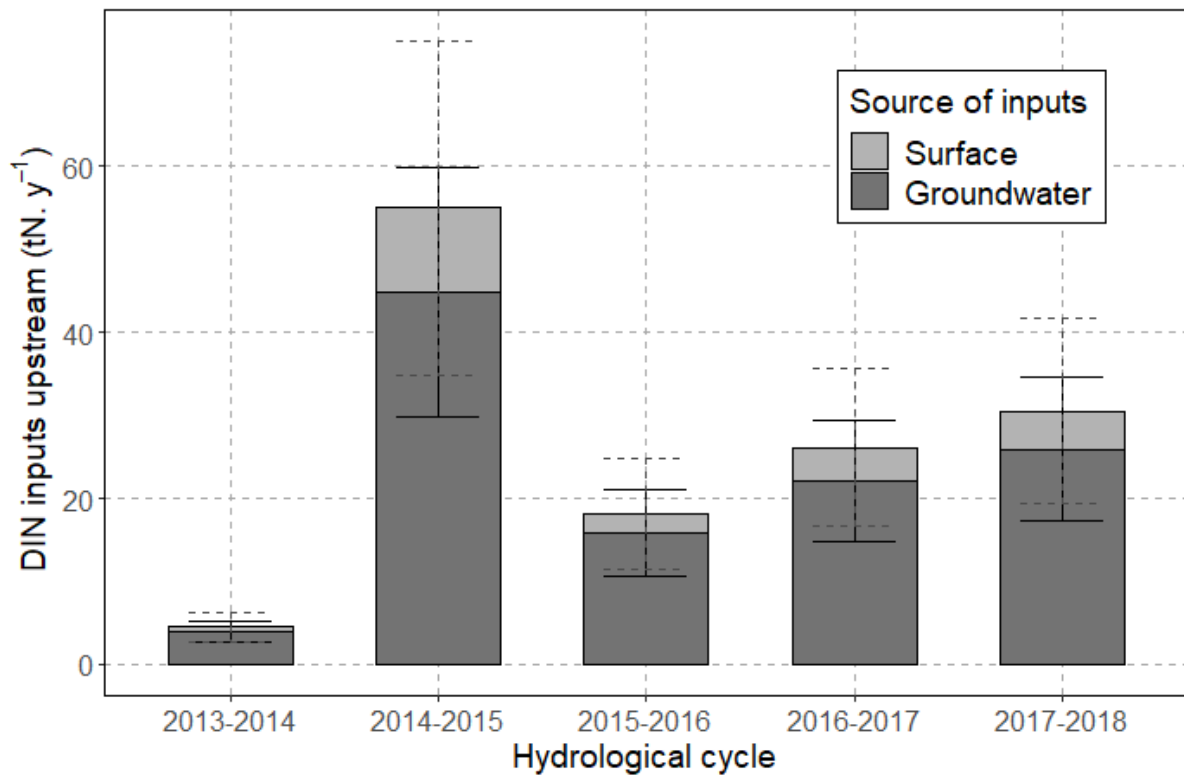


**Figure 4:** DIN inputs at the gauging station assessed from the flow interval method with data from Salaison gauging station monitoring (combining all sources), and groundwater contribution to the total DIN inputs estimated from baseflow separation and end-member mixing analysis (dark grey).

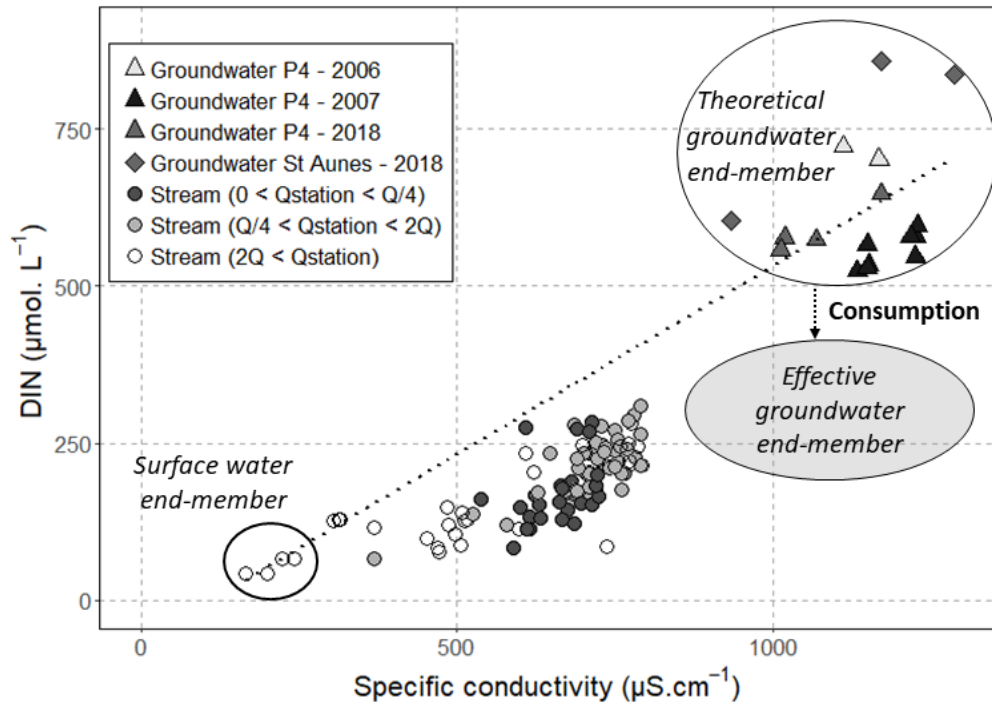


**Figure 5:** DIN evolution ( $\mu\text{mol}\cdot\text{L}^{-1}$ ) according to specific conductivity ( $\mu\text{S}\cdot\text{cm}^{-1}$ ) measured at Salaison gauging station from 2013 to 2018 (circles) for different water flow classes (in  $\text{L}\cdot\text{s}^{-1}$ ) (detailed in Table 2), and in the piezometer P4 in 2006, 2007 and 2018 (triangle) and in the piezometer St Aunes in 2018 (diamond). Dotted black line represents the hypothetical conservative mixing line between high conductivity/high DIN end-member and low conductivity/low DIN end-member.

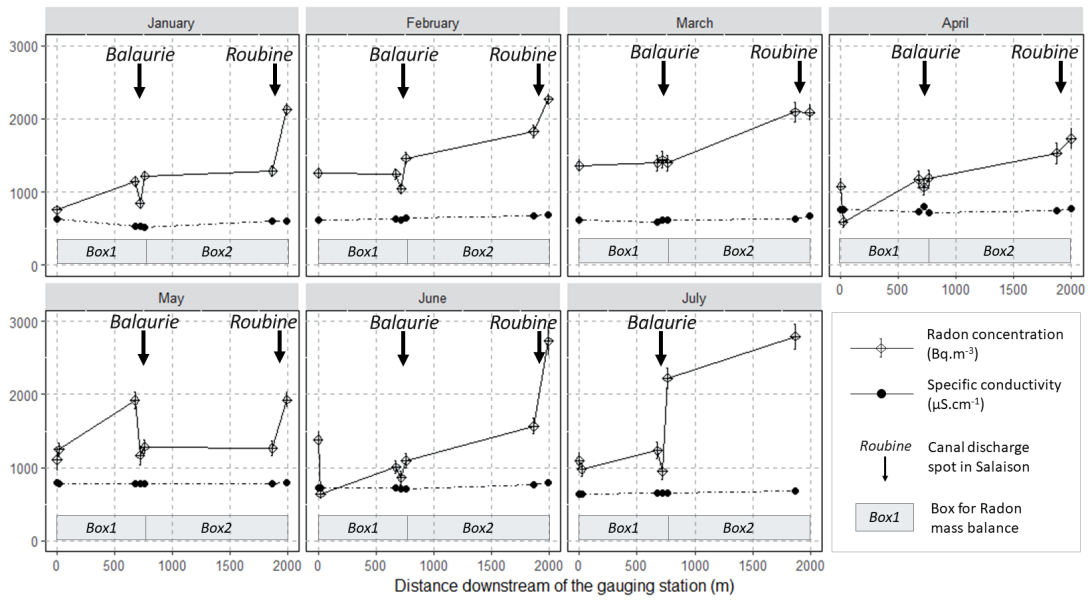


**Figure 6:** Radon concentration ( $\text{Bq.m}^{-3}$ ) and specific conductivity ( $\mu\text{S.cm}^{-1}$ ) in the downstream part of the river measured during each campaign in 2018. Grey boxes show the extent of radon mass balance implemented.

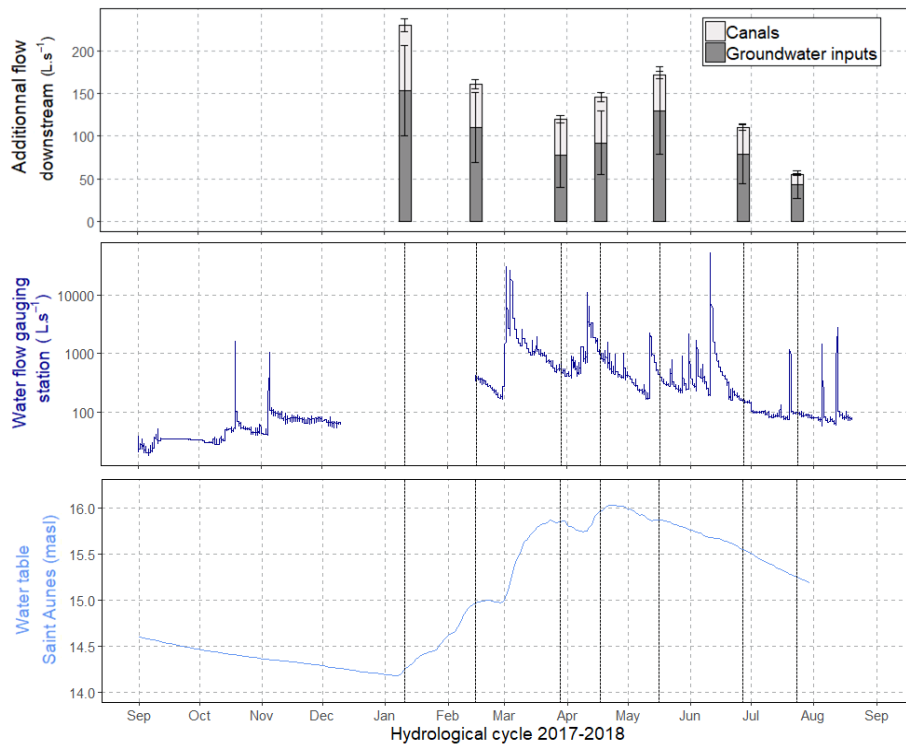


**Figure 7:** Groundwater discharge in the downstream part of Salaison River ( $L.s^{-1}$ ) assessed with the radon mass balance in 2018 (top); water flow at Salaison gauging station ( $L.s^{-1}$ ) (middle); water table fluctuation (m) at Saint Aunes piezometer (bottom). Vertical lines show campaign periods.



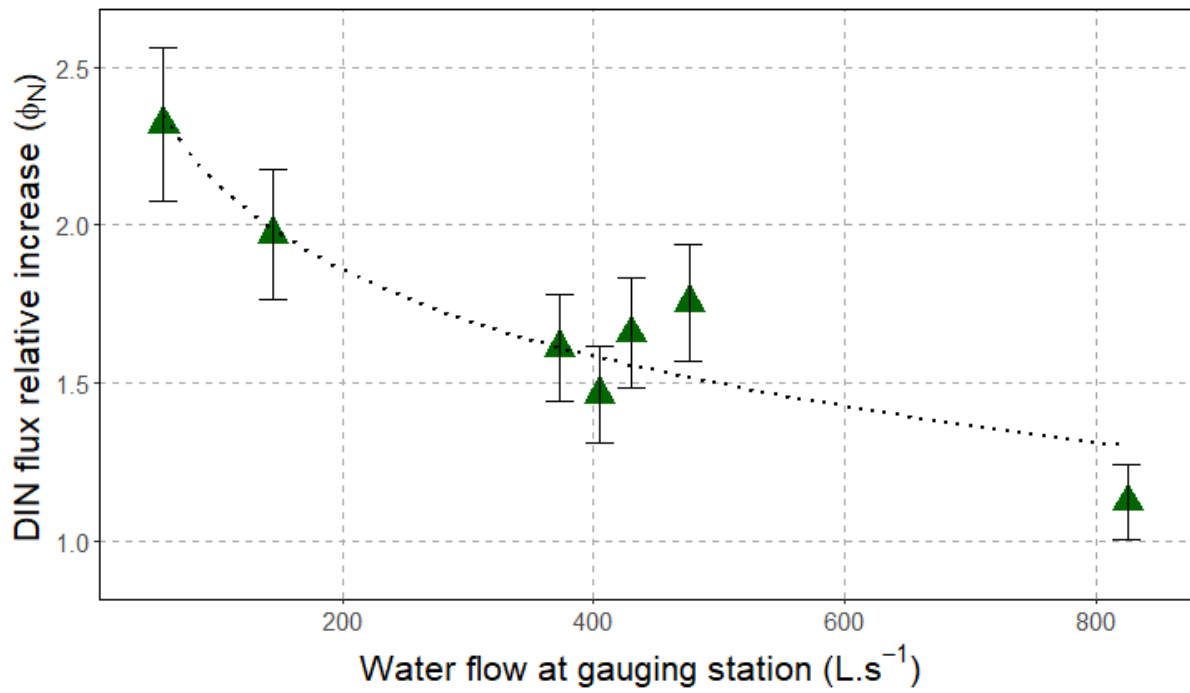


**Figure 8:** Increase factor of DIN flux downstream from the gauging station according to hydrological conditions at the gauging station (L.s<sup>-1</sup>).

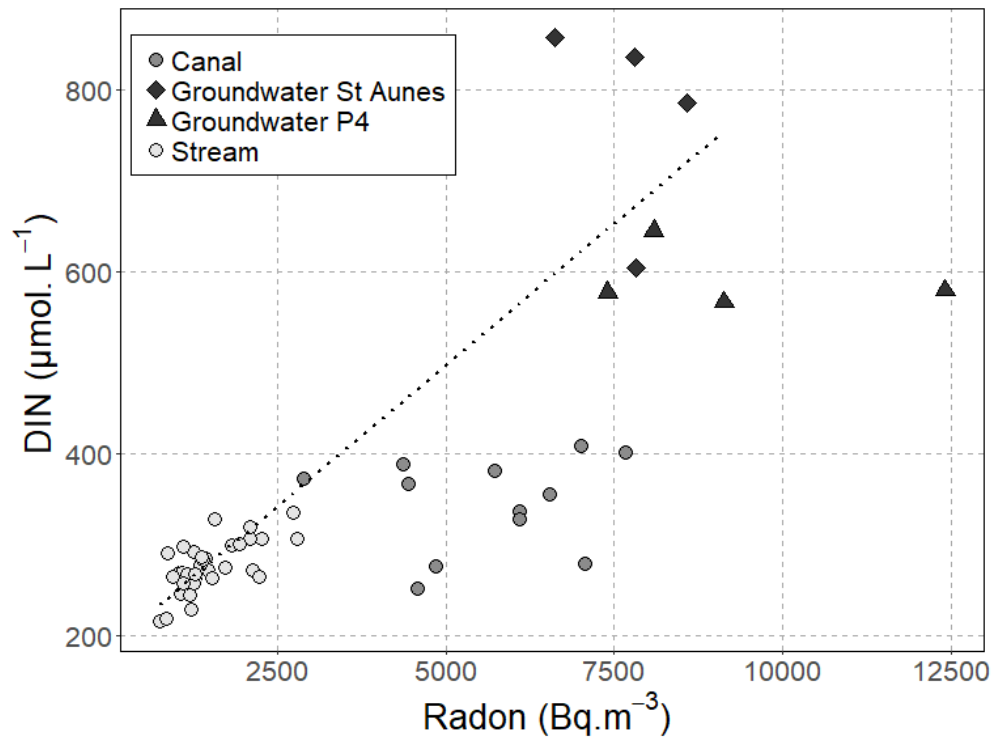


**Figure 9:** DIN concentrations ( $\mu\text{mol.L}^{-1}$ ) according to radon concentration ( $\text{Bq.m}^3$ ) in the downstream part of Salaison river measured during each campaign in 2018 in the stream (filled circles), in the two canals (hollow circles) and in piezometer P4 (diamonds).

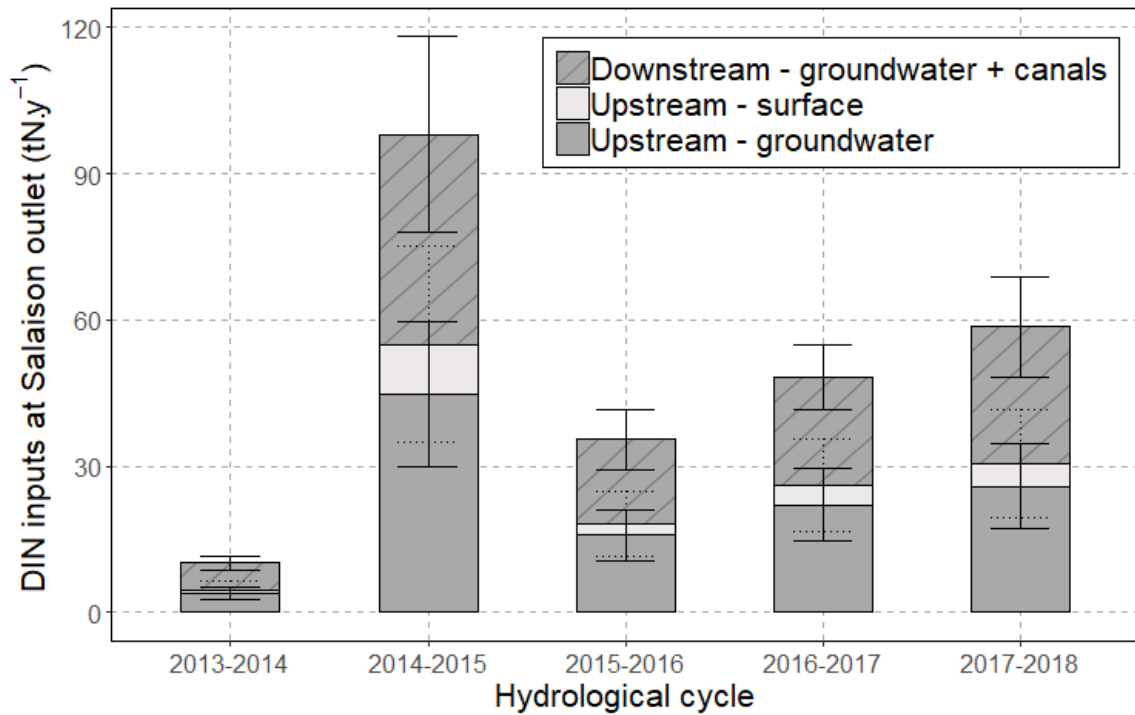


**Figure 10:** Estimation of DIN inputs to Or lagoon at Salaison outlet: upstream inputs estimated at the gauging station integrating groundwater-driven DIN inputs (dark grey) and surface-driven DIN inputs (light grey); additional groundwater-driven DIN inputs discharging downstream of the gauging station in the river and through the canals (dark grey with oblique lines).

		<b>Upstream</b>	<b>Downstream</b>
<b>Total DIN flux</b>	Waterflow	Data available at the gauging station from 2013 to 2018 - $Q_{station}$	Radon mass balance – $\Delta Q_{downstream}$ (Table 3, fig. 6 and 7)
	DIN concentration	Data available at the gauging station from 2013 to 2018 – $[N]_{station}$ (Fig 5)	Field sampling (Fig 9)
<b>Groundwater driven DIN flux</b>	Groundwater flow	Baseflow separation - $Q_{gw}$	Radon mass balance - $\Delta Q_{gw}$ (Table 3, fig. 6 and 7)
	DIN groundwater end-member	Conductivity/DIN correlation– $[N]_{gw\_s}$ (Fig 5)	Radon/DIN correlation – $[N]_{gw\_d}$ (Fig 9)

**Table 1:** Review of the different methods implemented to study DIN inputs in Salaison River. For each variable, the table presents the origin of the data, the variable name in the study (in bold) and the associated figures showing the data.

<b>Water flow class</b>	<b>Average DIN (<math>[N]_{\text{station}}</math>) (<math>\mu\text{mol.L}^{-1}</math>)</b>	<b>Standard deviation (<math>\mu\text{mol.L}^{-1}</math>)</b>
$0 < Q_{\text{station}} < Q/4$	$\mu = 170$	$\sigma = 62$
$Q/4 < Q_{\text{station}} < 2Q$	$\mu = 220$	$\sigma = 64$
$2Q < Q_{\text{station}}$	$\mu = 110$	$\sigma = 59$

**Table 2:** Flow classes and associated average DIN concentrations (source: DREAL) to estimate total nitrogen flux on the upstream part of Salaison river. Classes for each high-frequency water flow ( $Q_{\text{station}}$ ) were determined according to average water flow  $Q$  ( $386 \text{ L.s}^{-1}$ ) at the gauging station.

		January		February		March		April		May		June		July			
		Box 1	Box 2	Box 1	Box 2	Box 1	Box 2	Box 1	Box 2	Box 1	Box 2	Box 1	Box 2	Box 1	Box 2		
<b>Radon sources</b>	Inflow upstream	Water flow $Q_{in}$ ( $L.s^{-1}$ )	476	529	430	480	405	425	825	854	371	408	145	155	58	87	
		Radon concentration $C_{in}$ ( $Bq.m^{-3}$ )	756	1217	1255	1463	1354	1393	1075	1190	1107	1285	1378	1096	1095	2224	
	Inflow from canal	Water flow $Q_{can}$ ( $L.s^{-1}$ )	19	58	12	39	10	32	12	42	9	31	12	19	12	-	
		Radon concentration $C_{can}$ ( $Bq.m^{-3}$ )	4842	4358	6545	7665	6095	7016	4842	4358	6094	2883	4569	4441	2299	-	
	Diffusion from sediments	Diffusion flux $F_{diff}$ ( $Bq.m^2.s^{-1}$ )	6,9E-03	6,9E-03	6,9E-03	6,9E-03	6,9E-03	6,9E-03	6,9E-03	6,9E-03	6,9E-03	6,9E-03	6,9E-03	6,9E-03	6,9E-03	6,9E-03	6,9E-03
		Sediment surface $S$ ( $m^2$ )	5410	11888	6705	12093	5182	12093	6553	12217	6401	12093	5029	11229	5029	6205	
	Inflow from groundwater	Water flow $Q_{gw}$ ( $L.s^{-1}$ )	model output														
		Radon concentration $C_{gw}$ ( $Bq.m^{-3}$ )	8087	8087	8087	8087	9132	9132	9132	9132	9158	9158	10212	10212	12411	12411	
<b>Radon sinks</b>	Decay	Decay constant $\lambda$ ( $s^{-1}$ )	2,1E-06	2,1E-06	2,1E-06	2,1E-06	2,1E-06	2,1E-06	2,1E-06	2,1E-06	2,1E-06	2,1E-06	2,1E-06	2,1E-06	2,1E-06	2,1E-06	
		Box water volume $V$ ( $m^3$ )	2324	8699	3227	8884	2389	8885	3383	9378	5819	8885	1955	5430	1955	2742	
		Average Radon concentration ( $Bq.m^{-3}$ )	987	1671	1359	1864	1374	1741	1133	1460	1196	1606	1237	1913	1660	2509	
	Atmospheric evasion	Evasion coefficient $k$ ( $m.s^{-1}$ )	2,5E-05	2,5E-05	1,6E-05	1,6E-05	2,3E-05	2,3E-05	1,9E-05	1,9E-05	2,5E-05	2,5E-05	1,9E-05	1,9E-05	1,9E-05	1,9E-05	
		Water surface $A$ ( $m^2$ )	4648	9666	5867	9872	4343	9872	5638	9872	5639	9872	4343	9872	4343	4986	
		Average Radon concentration ( $Bq.m^{-3}$ )	987	1671	1359	1864	1374	1741	1133	1460	1196	1606	1237	1913	1660	2509	
	Outflow downstream	Water flow $Q_{out}$ ( $L.s^{-1}$ )	model output														
		Radon concentration $C_{out}$ ( $Bq.m^{-3}$ )	1217	2124	1463	2264	1393	2088	1190	1729	1285	1927	1096	2730	2224	2793	
<b>Radon mass</b>		<b>Water flowing out <math>Q_{out}</math> (<math>L.s^{-1}</math>)</b>	<b>529</b>	<b>654</b>	<b>480</b>	<b>591</b>	<b>425</b>	<b>526</b>	<b>854</b>	<b>971</b>	<b>408</b>	<b>545</b>	<b>155</b>	<b>255</b>	<b>87</b>	<b>113</b>	
<b>balance</b>		<b>Groundwater discharge <math>Q_{gw}</math> (<math>L.s^{-1}</math>)</b>	<b>34</b>	<b>119</b>	<b>38</b>	<b>73</b>	<b>10</b>	<b>69</b>	<b>17</b>	<b>76</b>	<b>26</b>	<b>106</b>	<b>-2</b>	<b>80</b>	<b>17</b>	<b>26</b>	
<b>outputs</b>																	

**Table 3:** Sources and sinks of the radon mass balance used in each campaign of this study. Water inflow in box 1 presented here corresponds to the manual measurements at the gauging station; diffusion from sediment was estimated in one sampling and the same value were applied in each

campaign; atmospheric evasion was evaluated at each campaign; groundwater radon concentrations corresponds to the nearest radon measurements made in P4 piezometer.